Rapid prey capture learning drives a slow resetting of network activity in rodent binocular visual cortex

Daniel P. Leman[1], Brian A. Cary[1], Diane Bissen[1], Brian J. Lane[1], M. Regis Shanley[1], Nicole F. Wong[1], Krish B. Bhut[1], Gina G. Turrigiano[1,2]

1. Department of Biology, Brandeis University, Waltham, MA 02453, USA
2. Corresponding author, contact: turrigiano@brandeis.edu

Keywords

Prey capture, cricket hunting, naturalistic learning, visual cortex, firing rate set point, dendritic spine, TNFα, homeostatic plasticity

SUMMARY

Neocortical neurons possess stable firing rate set points to which they faithfully return when perturbed. These set points are established early and are stable through adulthood, suggesting they are immutable. Here we challenge this idea using an ethological vision-dependent prey capture learning paradigm in juvenile rats. This learning required visual cortex (V1), and enhanced tuning of V1 neurons to specific behavioral epochs. Chronic recordings revealed a slow, state-dependent increase in V1 firing that began after learning was complete and persisted for days. This upward firing rate plasticity was gradual, gated by wake states, and in L2/3 was driven by a TNFα-dependent increase in excitatory synapses onto pyramidal neurons – all features of homeostatic plasticity within V1. Finally, TNFα inhibition after learning reduced retention of hunting skills. Thus, naturalistic learning in juvenile animals co-opts homeostatic forms of plasticity to reset firing rate setpoints within V1, in a process that facilitates skill consolidation.

INTRODUCTION

Experience-dependent plasticity in young mammals is essential for the proper wiring and functional maturation of neocortical circuits[1]. This process of circuit refinement requires cooperation between Hebbian forms of plasticity that use correlated or decorrelated activity to strengthen or weaken specific connections, and homeostatic forms that regulate excitability to stabilize firing and other network features around set point values[2]. In visual cortex, this interplay has been extensively studied using sensory deprivation paradigms, where closing one eye induces a drop in firing that is then slowly restored to baseline, through the sequential induction of Hebbian and homeostatic plasticity[3–5]. These ‘firing rate setpoints’ are evident at both the individual neuron and network level, established early in postnatal development, and

stable across time[3,4,6–11]. An outstanding question is whether these setpoints – once established – are truly invariant, or if they can be modulated or reset by salient experiences.

Prey capture learning is an ideal paradigm for testing this possibility. Rodents are opportunistic omnivores[12,13] and hunt insects for food in the wild[14–16] and in the lab[17–21]. While the drive to hunt is instinctive, rodents must practice to become proficient; in both adult and juvenile mice, the time to capture prey decreases by about an order of magnitude across repeated hunting bouts[21–23], presumably due to sensorimotor plasticity that enhances the ability to detect, track, intersect, and grasp prey. Binocular vision is the primary sense that guides the detection and pursuit of prey in rodents,[17,18,20,22,24,25] and prey capture learning enhances spine density and dynamics within L5 of mouse binocular primary visual cortex (V1b)[23], but whether this learning perturbs firing rate setpoints within V1b is unknown.

To address this, we obtained chronic extracellular recordings from upper layers of V1b of juvenile (critical period, CP) Long Evans rats before, during, and after they learned to hunt live crickets. Learning was rapid, prevented by chemogenetic inhibition of V1, and accompanied by a dramatic increase in the proportion of V1b neurons with firing strongly tied to the behavior. Firing rates in V1b were stable prior to and immediately after learning but began to slowly increase a few hours later and roughly doubled by ~60 hours post-hunting. This increase in network excitability was slow, accompanied by a TNFα-dependent increase in excitatory synapses onto L2/3 pyramidal neurons, and occurred primarily during active wake states, all signatures of upward homeostatic synaptic plasticity[1,3–5,26–32]. Finally, disrupting TNFα signaling post-learning impaired the retention of hunting skills. These findings suggest ethologically relevant learning initiates a slow transition to a new V1 network setpoint, that is driven by homeostatic forms of plasticity and enhances skill retention. Therefore, homeostatic activity setpoints are themselves substrates for experience-dependent plasticity.

Results

Prey capture learning is rapid and requires visual cortex

To determine whether vision-dependent learning can induce long-lasting changes in V1 activity, we designed a behavioral chamber that can be converted between “hunting” and “home cage” configurations to enable behavioral testing while allowing continuous, multiday video monitoring

and electrophysiological recordings before, during, and after learning. “Hunting” configuration (Figure 1A) features 4 Arduino-controlled dispensers that dispense individual live crickets in randomized order (Methods;[21,23]). “Home cage” configuration (Figure 1B) includes bedding, nesting materials, food and water *ad libitum*, and an adjacently housed littermate for social interaction. We then developed a single-day learning paradigm consisting of 3 hunting sessions, comprised of 10 hunts each, with 1.5-hour rest periods between sessions (Figure 1C). Prior to hunting, rats underwent two days of habituation and were fed immobilized crickets to overcome neophobia[21]. When first presented with live crickets, naïve rats were highly motivated to pursue but had difficulty successfully intercepting and capturing crickets (Figure 1D, top, Movie S1); however, they rapidly improved, and by the third session were much faster (Figure 1D, bottom, Movie S2). Quantification of capture times revealed a significant improvement across sessions (Figure 1D,E). There was no significant difference between males and females (Figure S1A), so data were combined, and both sexes were used for all subsequent experiments. To determine whether improved performance was due to faster initiation or shorter pursuits, we measured latency to attack (from release to pursuit initiation) and pursuit duration (from initiation to capture) for each hunt and found that both measures decreased significantly as learning progressed (Figure 1F,G).

Vision is the dominant sensory modality used during prey capture in rodents[17–25,33], but whether primary visual cortex (V1) plays an essential role is unknown. To test this, we inactivated V1 using viral expression of a Cre-recombinase (Cre)-dependent excitatory DREADDs construct (AAV9-hSyn-DIO-hM3Dq-mCherry) in V1, targeted to Parvalbumin-positive (PV) interneurons using transgenic PV-Cre rats[34] (Figure 1H). Clozapine-N-Oxide (CNO, 0.05mg/ml) was administered to rats via drinking water[35,36] for approximately 16 hours prior to hunting session 1 and between subsequent sessions; control animals were Cre^- littermates that received identical virus injection and CNO administration. To confirm this paradigm reduced V1 activity, we sacrificed rats following hunting session 3 and immunolabeled V1 slices for NeuN (to label pyramidal neurons)[36–38] and the immediate early gene cFos. We observed a significant decrease in the fraction of $NeuN^+$ neurons that were also $cFos^+$ in Cre^+ compared to Cre^- littermates (Figure 1I), indicating a robust reduction of V1 activity. Next, we compared hunting performance; Cre^- animals decreased time to capture across sessions as expected, and by session 3 rapidly caught prey (Figure 1J,S1B, Movie S3). In contrast, Cre^+ rats took ~3.5 times longer on average (Figure 1K,L, Movie S4), and failed to improve across sessions (Figure S1B).

Thus, V1 plays a critical role in mediating this visually-guided behavior and is required for rapid prey capture learning.

The activity of V1b neurons becomes tuned to behavior during prey capture learning

To determine whether vision-dependent naturalistic learning drives changes in the activity of V1 neurons, we recorded single-unit activity in layers 2/3 and 4 (L2/3, L4) of V1b continuously for 7 days in freely behaving juvenile rats, as described previously[3,6,36]. We targeted V1b because rodents use binocular vision to guide predation[17,18,20,22,24,25], and upper layers because of extensive information known about homeostatic mechanisms and firing rate homeostasis in L2/3 and 4[3–6,35,36,39–42]. Recordings were initiated during habituation (P26 or 27), maintained during learning (P28 or 29), and continued for 66 hours following the last hunting session (Figure 1C). We isolated regular spiking (RSU, predominantly excitatory neurons) and fast-spiking (FSU, putative inhibitory interneurons) single units as previously described[3,4,6,36,43,44], Methods). Control animals underwent the same paradigm as hunting counterparts (including receiving immobilized crickets during habituation), except in “sham” hunting sessions the cricket dispensers were empty, and rats were given a food pellet at the end of the session.

To assess if V1b activity becomes tuned to specific behavioral epochs during learning, we isolated individual RSUs that we could follow across all three prey capture learning sessions. We segmented each hunt into 4 epochs: inter-cricket interval (“ICI”, from consumption end to next cricket dispensation), latency to attack, pursuit duration, and consumption (from capture to the end of eating) (Figure 2A,B). Initially, most RSUs were not significantly modulated by hunting (Figure 2C, top), but as learning progressed, many RSUs developed robust responses to specific epochs, such as during pursuit (Figure 2C, bottom, red arrows). To quantify this, we calculated the percent change in firing for each neuron and took the population average (117 neurons, 6 animals) during pursuit and consumption epochs across sessions. RSU firing increased slightly during pursuits in hunting session 1 (Figure 2D, left), and the magnitude increased to ~50% during sessions 2 and 3 (Figure 2D, left). In contrast, during consumption epochs, RSU firing shifted from small net negative to small net positive across sessions but was not statistically significant (Figure 2D, right).

To determine what fraction of neurons became responsive during hunting, we compared firing rates during specific behavioral epochs to bootstrap shuffled firing rates for each neuron across sessions (Figure 2E). Many neurons that were initially unresponsive became significantly

modulated by pursuit as learning progressed; an example is shown in Figure 2F. Across the population, there was a progressive increase in the number of pursuit-responsive RSUs across hunting sessions, with ~40% significantly modulated by hunting session 3 (Figure 2G, top) and a similar increase in consumption-responsive RSUs (Figure 2G, bottom). Some RSUs were responsive to both pursuit and consumption, and this population also increased significantly across learning (Figure S2A). Finally, aligning firing to the beginning (Figure 2H, left) or end (Figure 2H, right) of pursuit epochs revealed greater activity in the responsive compared to the nonresponsive population, with the strongest modulation occurring after initiation of pursuit and preceding capture. Taken together, these data demonstrate that prey capture learning drives dramatic and widespread changes in V1b activity that are tied to specific behavioral epochs.

Prey capture learning induces a slowly developing and persistent increase in V1b firing rates

We next investigated whether vision-dependent learning modulates firing rates on a longer timescale. We compared RSU firing rate distributions at baseline and several days after learning (60 hours post-hunting). As expected, there was no significant difference between baseline distributions from hunt and sham animals (Figure 3A). Surprisingly, at 60 hours post-hunting, the distribution shifted significantly toward higher firing rates relative to the sham condition (Figure 3B), most prominently at the low end of the distribution (Figure 3C).

To determine how this shift develops, we followed individual RSUs as described previously[3,6,36] by spike-sorting our continuously-recorded dataset and identifying neurons that we could reliably track throughout the experiment (Figure 3D,E). Two examples of continuously recorded neurons are shown in Figure 3E; both underwent a slow increase in firing that commenced several hours after hunting session 3 and remained elevated well-above baseline by 60 hours post-hunting. The same pattern was seen in the normalized RSU population average, where firing slowly increased, with a pronounced light/dark oscillation, until roughly doubling by 50-60 hours post-hunting (Figure 3F,G; 45 neurons from 6 animals). Across the population, the majority of RSU firing rates significantly increased (Figure 3G), with about 2/3 of neurons increasing (Figure S3A) and 1/3 decreasing (Figure S3B). To determine whether this behavior depends on initial firing rates, we divided RSUs into terciles by baseline firing rates and plotted percent change at 60 hours post-hunting. Low firing rate neurons underwent the largest change, while high firing rate neurons changed the least (Figure 3H), consistent with our findings that the

firing rate distribution increased most at the low end (Figure 3C). In contrast to the dramatic, long-lasting changes in hunt firing rates, sham hunting produced only a transient change that returned to baseline by 60 hours (19 neurons from 6 animals, Figure S3C). Surprisingly, neurons recorded from monocular V1 (V1m) also showed no significant change in firing following hunting (12 neurons from 4 animals, Figure S3D), suggesting this effect is confined to V1b. Taken together, these data demonstrate that prey capture learning drives a gradual, long-lasting perturbation of V1b excitatory firing rates, that manifests both at the population level and in the activity of individual neurons.

Fast spiking firing rates slowly increase after prey capture learning

Increased RSU firing rates post-hunting could arise through a reduction in firing of inhibitory neurons. We therefore identified putative inhibitory fast-spiking units (FSU) based on spike waveform parameters (Figure 4A,[3,4,43,44]; Methods) and analyzed their activity. Like RSUs, FSU firing rates (41 neurons from 6 animals) increased during pursuit epochs, although not statistically significantly (Figure 4B, left), with no change during consumption (Figure 4B, right). The number of pursuit-responsive FSUs increased slightly during learning (Figure 4C), and like RSUs, the strongest modulation of FSU firing was at pursuit initiation and prior to capture (Figure 4D). Therefore, prey capture learning drives similar changes in RSUs and FSUs, suggesting a wide-spread reconfiguration of V1b response properties.

Next, we investigated whether prey capture learning triggers long-term changes in FSU firing rates, as it does for RSUs. Across FSUs we could follow continuously (28 neurons from 6 animals), we observed a slowly developing increase in the mean normalized firing rate that persisted for at least 60 hours post hunting (Figure 4E). Like RSUs, comparing baseline to 60-hour post-hunt also revealed a significant increase in FSU population firing rates (Figure 4F, left), with approximately 2/3 increasing (Figure 4F, middle) and 1/3 decreasing (Figure 4F, right). Thus, reduced FSU firing cannot account for increased RSU firing; instead, prey capture learning produces gradual, long-lasting changes in the activity of both excitatory and inhibitory circuit elements.

Upward regulation of FR post-learning is gated by sleep/wake states

This gradual increase in network excitability (Figure 3F,4E) is reminiscent of a slow homeostatic process, raising the interesting possibility that learning may rapidly “reset” activity setpoints

within V1b, and subsequently set in motion a slow transition to these new setpoints. Further, sensory-driven firing rate homeostasis is gated by sleep/wake states, and the strong light/dark oscillation in post-hunting firing rate increases (Figure 3F,4E) suggests this process could be similarly gated, since juvenile rats sleep more in the light and less in the dark[45]. To test this, we classified behavioral states of each animal into active wake (AW), quiet wake (QW), rapid eye movement (REM) sleep, and non-REM (NREM) sleep, using polysomnography[3,6,45]. Because longer periods of sleep or wake drive stronger firing rate homeostasis[3,6], we identified extended episodes of sleep and wake, and analyzed firing rate changes within those episodes (>30 mins in state[6,46]); REM episodes were excluded because they are generally short and there were too few extended episodes to reliably analyze.

In Figure 5A, the population average firing rates from one hunt animal is shown color-coded by behavioral state; during wake, there was a clear increase in firing, while during sleep, there was a subtle decrease. To quantify this across animals, we calculated the z-scored change in firing across sleep/wake episodes for each state (AW, QW, NREM). In hunt animals, the largest increase was during AW, with a smaller increase in QW and a small decrease in NREM (Figure 5B, left). In contrast, there was no significant increase during wake states in sham animals, and a small decrease during NREM (Figure 5B, right), consistent with the subtler, transient change in network activity in this condition (Figure S3C). In addition, for hunt (Figure 5C), but not sham (Figure 5D) animals, the longer they spent in a state, the larger the change. There was no difference in the proportion of time spent in individual behavioral states between hunt and sham conditions, in either light (Figure S4A, top) or dark (Figure S4A, bottom) periods. Thus, the post-learning increase in firing rates is specific to wake states and largest in AW, and the magnitude of change correlates with time spent in that behavioral state.

To determine whether the gradual stabilization of firing rates was reflected in the temporal profile of behavioral state-driven firing rate plasticity, we separately analyzed extended states at early (12hr), middle (36hr), and late (60hr) post-hunting timepoints. The largest percentage increase in firing during wake occurred in the middle timepoints, and by the late timepoint, wake no longer produced a significant increase and was balanced by a decrease during NREM (Figure 5E); results were similar when we analyzed z-scored firing rate (Figure S4B). Finally, to verify that wake-gated increases in firing were sustained regardless of subsequent behavioral state, we computed the change in firing rates at the end of the experiment (52-64 hours post-hunt) separately for each state and found similar increases (Figure 5F). In sum, after learning,

RSU firing rates increase incrementally across many periods of active wake. Because upward firing rate homeostasis is also gated by active wake[3,36] these data support the idea that this slow increase in network excitability is driven by homeostatic forms of plasticity.

Learning drives a TNFα-dependent increase in synapse number onto L2/3 pyramidal neurons that is necessary for the retention of hunting skills

Homeostatic forms of plasticity in V1 include changes in excitatory synaptic strength and number, as well as intrinsic excitability,[5,6,32,35,39,47,48] and are dependent on TNFα signaling[27,28,31,49–51]. To investigate the cellular basis of increased firing rates after learning, we used an *ex vivo* approach where animals were sacrificed 60 hours post-hunt or sham, and slices were prepared for whole cell recordings from V1b (Figure 6A,D). We focused on L2/3 pyramidal neurons because our chronic recordings encompass L2/3, and much is known about the expression of synaptic plasticity in this cell type[6,35,39]. We first probed excitatory quantal amplitude by recording miniature excitatory post-synaptic currents (mEPSCs) from L2/3 pyramidal neurons. Interestingly, we saw a small decrease in amplitude in hunt vs. sham animals (Figure 6A,B), accompanied by increased decay kinetics without changes in passive properties (Figure S5A-C), which suggests changes in synapse placement and electrotonic filtering of events measured somatically. Next, we performed whole-cell current-clamp recordings and generated frequency vs. current (F-I) curves in the presence of synaptic blockers, which revealed overlapping F-I curves (Figure 6 E,F), and no significant difference in rheobase, input resistance, or area under the F-I curve (Figure 6G-I). Thus, increased firing of L2/3 pyramidal neurons is not driven by a net increase in excitatory quantal amplitude or enhanced intrinsic excitability.

Changes in excitatory synapse number are another major expression locus of homeostatic plasticity in V1 pyramidal neurons[5,27,41,48,52], and prey capture enhances synapse density in the output layer (L5) of V1[23]. To determine whether changes in excitatory synapse number could account for enhanced firing in L2/3, we quantified dendritic spines as a proxy for excitatory synapses. We utilized a Thy1-YFP mouse line with sparse labeling in V1b L2/3 pyramidal neurons, which allowed for high-resolution reconstruction of entire dendritic arbors and accompanying spines (Figure 7A-C). Juvenile mice learn to hunt more slowly than rats[21,23], so we used a modified paradigm consisting of 1 sham or hunt session/day for 3 days, followed by an additional “probe” session 3 days later (Figure S6A, top[23]), then quantified spine density on

days 1 and 6. There was a significant increase in the cumulative distribution of spine density across all dendritic segments in hunt animals on day 6 (Figure 7D) but not day 1 (Figure S6C), indicating that learning induced a slow, robust, and widespread increase in spine density. The mean spine density was also significantly increased by ~25% (Figure 7D, inset, 6 neurons/condition). Consistent with decreased quantal amplitude (Figure 6B), there was a small but significant decrease in the cumulative distribution of spine head diameters after hunting (Figure 7E), which was not significant when calculated by cell (Figure 7E, inset). These data support the idea that post-learning spine formation generates a new population of smaller excitatory synapses in L2/3 pyramidal neurons.

Homeostatic forms of plasticity, including sensory-deprivation induced spine plasticity in V1, are sensitive to TNFα signaling[23,26,27,51], prompting us to ask if post-learning spine addition in L2/3 pyramidal neurons could be prevented by inhibiting this pathway. To answer this, we treated animals with XPRO1595 (XPro), a soluble TNFα scavenger that crosses the blood brain barrier and produces long-lasting inhibition of TNFR1 to block homeostatic plasticity[23,26,27,51]. We injected XPRO1595 immediately post-hunt or sham on day 1, again 3 days later, and on day 6 analyzed dendritic spine density and diameter onto L2/3 pyramidal neurons from V1b (Figure S6A, bottom). Strikingly, in the presence of XPro, spine density and diameter were not significantly different between hunt and sham conditions (Figure 7F,S6D); additionally, in the XPro condition, average spine density was similar to controls (Figure 7D and 7F, insets), suggesting XPro did not majorly impact baseline spine density.

If the persistent, learning-induced change in V1b spine density is important for consolidation or maintenance of skills, then preventing it with XPro should also degrade behavioral performance. Indeed, XPro-treated mice performed significantly worse during the probe hunting session than control (Figure S6B). Because retention can be cleanly separated from learning in our 1 day rat learning paradigm (Figure 1A), rats were injected with XPro or saline after the last hunting session on day 1 (when learning was complete) and tested 3 days later (“probe”, Figure 7G). Both cohorts of animals performed similarly during learning (Figure 7H); however, the XPro cohort performed significantly worse during the probe sessions (Figure 7I-L). XPro-treated rats had roughly double the time to capture as controls (Figure 7J), and latency to attack (Figure 7K) and the pursuit duration (Figure 7L), were longer. Thus, post-learning spine addition in L2/3 is mediated by a TNFα-dependent process, and loss of TNFα-dependent plasticity impairs the retention or consolidation of hunting skills.

DISCUSSION

The idea that cortical neurons and circuits express stable firing rate set points to which they faithfully return when perturbed has become well-established[3,4,6–8,10,11,53–55]. In neocortex these set points are evident early in postnatal development and are stable through adulthood[9–11], suggesting they are stable features of neurons and/or cortical circuits. Recent work has shown that activity setpoints in culture can be altered pharmacologically[54–56] but whether these setpoints are malleable *in vivo*, and can serve as a substrate for plasticity during naturalistic behaviors, was unknown. Here, we show that vision-dependent learning in juvenile rats induces a persistent resetting of visual cortical firing rates. First, we show rapid prey capture learning requires V1 and enhances the tuning of V1 neurons to specific hunting epochs. Chronic recordings before, during, and after this learning revealed a slow, state-dependent increase in baseline V1b firing rates began shortly after learning was complete and persisted for days afterwards. This slow increase in firing was gated by sleep/wake states, and in L2/3 pyramidal neurons was driven by an increase in spine density. Finally, inhibiting TNFα signaling post-learning both blocked spine addition and reduced the retention of hunting skills. The slow timescale, as well as dependence on behavioral state and TNFα signaling, implicate homeostatic forms of plasticity in driving these changes. These results suggest that naturalistic learning in young animals can co-opt homeostatic forms of plasticity to drive neocortical networks to new activity setpoints.

Prey capture in rodents is a complex behavior that requires cooperation between many brain regions and circuits[17–19,22,24]. Here, we focus on V1 because vision is the primary sense used to track and grasp prey[17,18,20,22,24,25], and we show that inactivating V1 prevents learning of this behavior. Multiple visual pathways likely cooperate to enable effective hunting; for example, the superior colliculus is important for the execution of hunting skills after animals become proficient[18], but whether this pathway undergoes learning-induced plasticity that contribute to behavioral improvement is unknown. In V1, we find that neural responses become strongly tuned to pursuit across a single day of hunting, demonstrating rapid functional plasticity correlated with performance. Interestingly, in critical period (CP) mouse V1, prey capture learning sharpens temporal frequency tuning but has little effect on other receptive field properties such as orientation tuning[23], suggesting the initial, rapid phase of V1 plasticity we observe is likely tied to enhanced tracking of moving prey and other, more holistic aspects of visuomotor processing. While our data strongly support a role for V1 plasticity in the acquisition

of hunting skills, they do not, of course, preclude contributions from plasticity in other brain regions.

Surprisingly, hunting induced the most dramatic changes in V1b activity after learning was complete. Despite animals returning to a home-cage environment with no further enrichment, both putative excitatory and inhibitory neurons underwent a slow increase in firing that persisted for at least 64 hours post-learning. This contrasts with chronic recordings from primary motor cortex in adult rats, where firing rates remained stable during and after motor learning[10,11], and from CP V1, where firing rates (and other activity measures) are restored to baseline within a few days of perturbations induced by passive sensory manipulations[3–7,29,36]. Like sensory deprivation, sham hunting induced only a transient change in firing before activity returned to baseline. This suggests naturalistic learning during the CP has a unique effect on neocortex that drives a slow movement of network activity away from the default set point to a new, higher activity regime. This plasticity was especially evident in slowly-firing neurons, so it may serve to move a population of low information-containing neurons into a firing regime where they can contribute more effectively to sensorimotor processing and integration[57]. Because our chronic recordings in these young, growing animals are limited in duration, we are unable to say whether this new activity state is permanent or merely long-lasting.

Homeostatic plasticity is generally understood to stabilize activity around an established activity setpoint[1,2,32,58]; in contrast, we find that after learning, network activity slowly moves away from the original setpoint to a new, higher activity state. If plasticity arises through a rapid resetting and then slow movement to this new setpoint, then this should unfold according to the rules and mechanisms of homeostatic plasticity. Both intrinsic and synaptic plasticity can contribute to firing rate homeostasis within V1[5,6,8,32,35,35,39], and expression of these cellular forms of plasticity[26,27,31,49,51,59], as well as the restoration of network activity[26–28] depend on TNFα signaling. Synaptic homeostasis can target both strength and number of synapses[32,42,47,48,58,60,61], and we find the density of excitatory synapses onto L2/3 pyramidal neurons increases with network activity in a TNFα dependent manner. As other forms of cortical synaptic potentiation, such as LTP, are insensitive to TNFα blockade[28,31], this strongly implicates homeostatic, rather than Hebbian, synaptic plasticity. On the other hand, unlike for deprivation-induced homeostatic regulation[35,39], intrinsic excitability of L2/3 neurons was not enhanced post-learning. These differences are consistent with previous work showing that which cellular homeostatic mechanisms are recruited depends on many factors, including when

and how the network is perturbed[40,51,61]. In sum, the synaptic changes set in motion in L2/3 after naturalistic learning are slow, widespread across the dendritic arbor (Figure 7D), and TNFα-dependent, all defining features of homeostatic synaptic plasticity.

The homeostatic nature of the post-learning firing rate increase is further supported by its behavioral state-dependence; like upward firing rate homeostasis induced by visual deprivation[3,36], the post-learning increase in firing accumulated incrementally across successive periods of wake. This contrasts with Hebbian potentiation in V1, which is either independent of sleep/wake states or occurs selectively during sleep[62–65]. Interestingly, memory consolidation in the hippocampus[62,66–71] (but see[72–75]) and some forms of experience-dependent plasticity consolidation in V1[62,65] occur preferentially during sleep states, whereas we find that consolidation is associated with net upward wake-dependent plasticity. Although the net effect on firing was upward, there was a pronounced oscillation in firing that was associated with cycles of wake-enrichment (up) and sleep enrichment (down), raising the possibility that wake-dependent and sleep-dependent mechanisms cooperate to reshape network activity as hunting skills are consolidation.

What function(s) might this resetting of network activity serve? By bringing very low firing rate neurons into a more functional firing rate regime, this process may better integrate these neurons into the local network and thus enhance sensory processing during complex behaviors. Additionally, this process might increase the population of neurons that are available as substrates for future learning. In insular cortex, homeostatic plasticity can enable the emergence of memory specificity after gustatory learning[76], suggesting that task-specific processing could be maintained or even enhanced during this resetting of network activity. Most broadly, this work shows that neocortical activity setpoints are malleable and suggests that learning-dependent changes in these setpoints contributes to behavioral improvements during naturalistic learning.

MATERIALS AND METHODS

Experimental model and subject details

All procedures were approved by the Brandeis University Institutional Animal Care and Use Committee and conformed to the National Institutes of Health *Guide for the Care and Use of Laboratory Animals*; colonies of rats and mice were maintained at Brandeis in the Foster

Biomedical Research Facility. For all experiments, rats and mice of both sexes were used. Rats were juvenile Long Evans (Charles River Laboratories, Cambridge, MA, USA) or Parvalbumin (Pvalb)-Cre on a Long Evans background[34], founder rats obtained from Loren Frank (University of California, San Francisco). Mice were Thy1-YFP (B6.Cg-Tg(Thy1-YFP)HJrs/J, The Jackson Laboratory, Bar Harbor, ME, USA), which express the yellow fluorescent protein (YFP) in a subset of L2/3 pyramidal neurons.

Rat prey capture learning paradigm

Littermate rats were transferred to behavioral testing rooms 2 days prior to cricket hunting. Rats were given standard housing, chow, and nesting materials as previously described[3,4,6,36]. A circadian light cycle of 12-hour light/dark periods was maintained, with dark hours between 7:30am and 7:30pm. All cricket hunting experiments took place in a behavioral testing arena as described previously[21,23]. Briefly, the behavioral arena consisted of a 14”x14”x14” plexiglass chamber with a removable floor with absorbent pad, social partner divider, and detachable cricket dispensers. In “home cage” configuration, rats were given *ad libitum* chow, water, bedding, and access to a social partner via a perforated, transparent divider (Figure 1B. In “hunting configuration,” the social partner was removed, chow, water, and nesting materials were removed, the floor was replaced with a clean pad, and cricket dispensers were affixed to the four corners of the arena (Figure 1A). Additionally, diagonal stripes were attached to the outside of the arena to provide visual distractors on all four sides of the testing arena. For two days, animals were handled by experimenters and acclimated to the behavioral arena in “hunting configuration” for 30 minutes and fed two live, but immobilized crickets each day. Crickets were sourced from Fluker Farms (Port Allen, LA, USA). On the second day of acclimation, immediately prior to lights out, rats were food deprived for no more than 16 hours. Behavioral testing began the next day, when the behavioral arena was configured into “hunting” mode and crickets were loaded into the cricket dispensers. Each hunting session consisted of a 5-minute baseline period prior to when the first cricket was dispensed. Crickets were dispensed using custom, in-house designed 3D printed dispensers controlled by custom Arduino-powered stepper motors and software. With each cricket hunt, dispensers on opposite sides of the arena were programmed to turn to prevent the animals from predicting which dispenser a cricket would be released from. Behavior was recorded at 20 frames per second using either a Logitech C922x HD Pro Webcam or an infrared-capable Sony IMX323 webcam, via Synapse (Tucker Davis Technologies (TDT), Alachua, FL, USA) software. Each hunting session consisted of 10 crickets and typically lasted 30-45 minutes. After each hunting session, the

arena was returned to “home cage” configuration. For all hunting experiments, rats performed 3 hunting sessions on Day 1. In a subset of experiments, animals performed a probe day of hunting 3 days later (Day 4), consisting of prior food deprivation and 2 hunting sessions. At the completion of the final hunting session of the day, animals were returned to *ad libitum* food and water access. On days where hunting did not occur, animals were housed in “home cage configuration.” Animals were sacrificed following the end of the behavioral paradigm in accordance with Brandeis Institutional Animal Care and Use Committee guidelines.

Mouse prey capture learning experiments

For mice prey capture experiments, we used the paradigm described in Bissen et al., [23], modified from Groves Kuhnle et al., [21], with the same arena configuration as for rats. Briefly, mice were transferred to behavioral testing rooms 2 days prior to the first day of hunting. Mice were handled and habituated for 1 hour and fed one live, but immobilized cricket per day. Mice were food deprived for up to 16 hours prior to the start of each hunting/sham session but had water ad libitum. Mice then underwent three days of one session per day of hunting/sham (days 1-3), followed by two days with no hunting/sham session (days 4-5) and one last day with one hunting/sham session (day 6). Each hunting session comprised 10 live crickets, while each Sham session comprised 10 immobilized crickets. All hunting/sham sessions took place over the course of 6 days between P28 and P35, with the first session taking place on P28-P30.

Chemogenetic (DREADDs) disruptions of Visual Cortex (V1)

Virus injections of excitatory DREADDs (AAV9-hSyn-DIO-hM3D(Gq)-mCherry, Plasmid #44361-AAV9, Addgene, Watertown, MA, USA) were performed on juvenile PV-Cre$^{+/-}$ and PV-Cre$^{-/-}$ rats ages P14-P18[34]. Rats were anesthetized with vaporized isoflurane (4-5% induction, 1-2% maintenance) via an integrated vaporizer (Somnosuite, Kent Scientific, Torrington, CT USA) connected to a stereotaxic holder (Model 923-B with Model 1924-C-11.5 mask, Kopf Instruments, Tujunga, CA. Two injection sites were chosen per hemisphere, and 200-300nL of virus was delivered into V1 via a micropipette and oil-hydraulic injector (MO-10, Narishige International USA, Amityville, NY, USA). Clozapine N-Oxide (CNO, HelloBio, Princeton, NJ, USA) was dissolved in water and 10mM saccharine chloride was added to reach a final concentration of 0.05mg/mL[36]. At lights out on the evening prior to hunting, rats’ drinking water was replaced with CNO-water, and access was given until the cessation of hunting session 3 the following day. Animals drank 15-20 mL over the course of administration to reach a desired CNO dose of 10 to 15 mg/kg[36].

Continuous-single cell recordings in freely behaving animals

Juvenile Long Evans rats (P22-P24) were implanted with electrode arrays as previously described [3,77,6,36]. In brief, custom 16 or 32-channel microwire arrays (tungsten, 33 micron diameter, Tucker Davis Technologies (TDT), Alachua, FL, USA) were implanted in either V1b or V1m (validated post-hoc). Rats were anesthetized with vaporized isoflurane (4-5% induction, 1-2% maintenance) via an integrated vaporizer (Somnosuite, Kent Scientific, Torrington, CA, USA) connected to a stereotaxic holder (Model 923-B with Model 1924-C-11.5 mask, Kopf Instruments, Tujunga, CA, USA). The skull was exposed via a small incision, cleaned with hydrogen peroxide, and bleeding spots were cauterized. Bone screws (Antrin Inc, Fallbrook, CA, USA) were implanted above the cerebellum posterior to bregma and bilaterally above motor cortex. V1b or V1m were located using stereotaxic coordinates and anatomical landmarks, and the bone was removed using a 27G needle. A headcap was created using UV-cured acrylic (Flow-It Flowable Composite, Pentron Technologies, Orange, CA, USA). The dura was removed using a 27G syringe and kept moist using chilled, bacteriostatic sterile 0.9% saline (Hospira Ince, Lake Forest, IL, USA). Electrodes were slowly lowered into the brain, and the craniotomy was encapsulated with a silicone elastomer (Kwik-Cast, World Precision Instruments, Sarasota, FL, USA). The electrode array was secured using additional UV-cured acrylic. A steel ground wire from the electrode array was then secured to one of the bone screws over motor cortex using solder paste and additional dental acrylic. Finally, a braided steel wire from the electrode array was implanted into the nuchal muscle for EMG recordings.

Following electrode implantation, animals were allowed to recover for at least 2 days with *ad libitum* access to food and water. During this time, animals were administered postoperative injections of meloxicam and penicillin during the first two days of recovery and were handled daily by experimenters. Animals were then transferred to our custom, convertible behavioral arena in the previously “home cage” configuration, and allowed to habituate to the arena for two days prior to initiation of hunting, as described above. The microwire arrays were connected to TDT commutators via ZIF-clip headstages that enable animals to move freely throughout the arena. Implanted animals were accompanied by a littermate social partner in the adjacent chamber in “home configuration.” Animals were continuously connected via an active commutator for the duration of the experiment and behavior was continuously recorded using an IR-capable camera, enabling constant recording of electrophysiology and behavioral data. Electrophysiology data was acquired at 25kHz and streamed using a TDT Neurophysiology

Workstation and Data streaming pipeline. Spike extraction, clustering, and sorting were performed using custom MATLAB and Python code as previously described [3,77,6,36].

Slice electrophysiology recordings

Rats were deeply anesthetized with isoflurane and rapidly decapitated. Brains were rapidly removed and sliced in ice cold, oxygenated artificial cerebrospinal fluid, (aCSF, in mM: 126 NaCl, 25 NaHCO3, 3 KCl, 2 CaCl2, 2 MgSO4, 1 NaH2PO4, 0.5 Na-Ascorbate, osmolarity adjusted to 315 mOsm with dextrose, pH 7.35) using a vibratome (Leica VT1200S). Slices were allowed to recover in oxygenated aCSF at 34°C for 1 hour prior to the start of recordings, then moved to room temperature. All recordings were performed within 6 hours of slicing. During recordings, slices were continuously perfused with oxygenated aCSF at 34°C. For intrinsic excitability recordings, aCSF contained synaptic blockers (in mM: 25 DNQX, 50 APV, 25 PTX) and used K-gluconate internal (in mM: 100 K-gluconate, 20 KCl, 10 HEPES, 5.37 Biocytin, 10 Na-Phosphocreatine, 4 Mg-ATP, and 0.3 Na-GTP, with sucrose added to bring osmolarity to 295 mOsm and KOH added to bring pH to 7.35). For spontaneous mEPSC recordings, aCSF contained synaptic blockers (APV and PTX) at the same concentrations above as well as TTX to block action potentials (0.2 uM) and used CS based internal (in mM: 115 Cs-Methanesulfonate, 10 HEPES, 10 BAPTA•4Cs, 5.37 Biocytin, 2 QX-314 Cl, 1.5 MgCl2 , 1 EGTA, 10 Na2 -Phosphocreatine, 4 ATP-Mg, and 0.3 GTP-Na, with sucrose added to bring osmolarity to 295 mOsm, and CsOH added to bring pH to 7.35). Slices were visualized on an Olympus BX51WI upright epifluorescence microscope using a 10x air (0.13 numerical aperture) and 40x water-immersion objective (0.8 numerical aperture) using infrared differential interference contrast optics and a CCD camera. Pyramidal neurons in L2/3 were targeted by the presence of an apical dendrite and a teardrop shaped soma and confirmed with post-hoc reconstruction using biocytin labeling. Glass pipettes were pulled using a Sutter P-97 to obtain a tip resistance between 3-6 MOhm. Data was acquired at 10 kHz using Multiclamp 700B amplifiers and CV-7B headstages (Molecular Devices, Sunnyvale CA), with MATLAB- based data acquisition software, WaveSurfer (v 1.0.5, Janelia, Ashburn VA). All post-hoc analysis was performed using custom scripts written in MATLAB (Mathworks, Natick MA).

Immunohistochemistry

Rat Immunohistochemistry

Animals were deeply anesthetized with a Ketamine/Xylazine/Acepromazine (KXA) cocktail (70 mg/kg ketamine; 3.5 mg/kg xylazine; 0.7 mg/kg acepromazine) and perfused with phosphate-

buffered saline (PBS) and 4% paraformaldehyde. Fixed brains were sliced at 60-micron thickness on a vibratome (Leica VT1200, Leica Biosystems, Deer Park, IL, USA) and stored in 1x PBS. For electrophysiology experiments, brains were stained with DAPI and imaged with an epifluorescence widefield microscope (Keyence BZ-X, Keyence, Woburn, MA, USA) to verify electrode location post-hoc. For DREADDs-manipulation experiments, slices were washed, incubated in a blocking solution for 2 hours, then incubated with primary antibodies: rabbit anti-cFos (9F6, Cell Signaling Technology) (1:200), rat anti-mCherry (M-11217, Invitrogen) (1:1000), and mouse anti-NeuN (MAB-377, Millipore Sigma) (1:500). The following day, slices were incubated with secondary antibodies: goat anti-mouse Alexa-488 (A-11001, Invitrogen), goat anti-rat Alexa-594 (A-11007, Invitrogen), and goat anti-rabbit Alexa-647 (A-21245, Invitrogen) (all 1:400). Images were obtained using a confocal microscope (Leica SP5, Leica Microsystems, Deer Park, IL, USA).

Mouse Immunohistochemistry

Animals were sacrificed a minimum 3 hours after the last hunting session on day 6 using the previously described methods. Mice were deeply anesthetized and perfused as for rats in the previous section. After dissection and post-fixation, brains were sectioned in 200µm thick slices to encompass complete dendritic trees. Selected slices with entire dendritic arborizations of L2/3 pyramidal neurons in V1b were permeabilized, blocked, and incubated with primary antibodies in blocking solution for 48-72 hours at 4 °C, and incubated with corresponding secondary antibodies for 2 hours at room temperature. Slices were stained with chicken anti-GFP (90890, MilliporeSigma) (1:500) and rabbit anti-NeuN (2736207, ThermoFisher) (1:500), followed by goat-anti-chicken Alexa 488 (143165, ThermoFisher) and goat-anti-rabbit Alexa 568 (143157, ThermoFisher) (both 1:500). Images were obtained using a confocal microscope (LSM 880, Zeiss, Oberkochen, Germany).

Pharmacological manipulations using XPRO1595

The pegylated protein tumor necrosis factor alpha (TNFα)-1 inhibitor XPro1595[78] (INmuneBio, Boca Raton, FL, USA) was administered as previously described[23,26,27,51,79]. XPRO1595 was dissolved in 0.9% saline to the desired concentration (1mg/mL). Animals were weighed and the appropriate amount of XPRO1595 was delivered via subcutaneous injection to reach the desired dosage (10mg/kg). For mice cricket hunting experiments, XPRO1595 was administered twice, once approximately one hour following the Day 1 hunting session, and again 3 days later, roughly halfway through the paradigm, after the Day 3 hunting session. The control cohort

consisted of non-injected (n=5) and saline-injected (n=3) mice; these two cohorts had similar learning curves (see[23]) and were therefore combined. For rat cricket hunting experiments XPRO1595 was administered to rats once, approximately one hour following the cessation of hunting session 3 on the first day of hunting. Animals were retested 3 days later on "Probe" day, consisting of 2 hunting sessions of 10 crickets/session.

QUANTIFICATION AND STATISTICAL ANALYSES

Prey capture learning Behavioral Scoring

Quantification of Hunting Performance

Behavior was recorded during each cricket hunting session were manually scored to quantify cricket entrance, the pursuit initiation, cricket capture, and end of consumption. Time to capture was calculated as the time (in seconds) from cricket entrance to capture. Latency to attack was calculated as the time from cricket entrance to pursuit initiation, and attack duration was calculated from pursuit initiation to capture. Further behavioral analysis was performed using DeepLabCut (DLC,[80,81]) to assess differences between conditions in DREADDs-manipulation experiments, as well as in XPRO1595 experiments. Over 300 still frames from hunting videos were chosen and manually labeled with cricket position and the position of various rat body features. As previously described[21,23], a ResNet50 neural network was trained on these manually labeled datasets. Following training, the performance of the network was evaluated using test data. Outlier frames were then chosen and manually labeled for subsequent training iterations to improve performance. DeepLabCut outputs of cricket position coordinates and rat head position were then used to create trajectories of cricket hunting pursuits using custom software (MATLAB).

Behavioral State Scoring

Behavioral state scoring was accomplished as previously described using a semi-automated MATLAB GUI[6] with the modification that animal movement was tracked using DLC[80,81]. Briefly, local field potentials were extracted from 3 of the highest quality channels, downsampled, and averaged. We computed the spectrograms in 5 second bins from 0.3 to 15 Hz. Standard delta (0.3 – 4 Hz) and theta (5 – 8 Hz) bands were used to differentiate cortical states. Animal movement was measured using downsampled mean EMG signal and DLC tracked body poses separate for the head and body of the animal. DLC poses were processed by first removing all low confidence points (<0.9 confidence). 8 head features were tracked (nose, ears, etc.) along

with 3 body features, allowing for separate head/body movement tracking. The instantaneous speed of each pose was calculated and smoothed with a 30 frame lowess function (MATLAB). The head and body speed were determined by taking the median speed of each pose. A trained human scorer used the GUI to manually score the first 10 hours of behavioral data, and then subsequently supervised the labeling of the rest of the experimental data with a random forest model trained on those first 10 hours (process was repeated for each animal).

Behavioral State Analysis

To measure sleep/wake effects on firing rates (FRs) we first detected extended sleep/wake episodes. Episodes were defined as periods of near-continuous (<120 second interruptions) sleep/wake lasting at least 30 minutes. To determine overall FR change (Figure 5B, E), we measured the difference in FRs in flanking windows located in the first 30% and last 30% of each episode. We calculated z-score change by first normalizing $zFR=(FR-\mu)/\sigma$, where μ (mean) and σ (standard deviation) were calculated based on the FR data only within the episode. Next, we found the mean change $FR_{last}- FR_{first}$ where both were mean FRs for the same given state in the flanking periods (Figure 5B). Percent change was calculated $\%change=100*(FR_{last}- FR_{first})/ FR_{first}$, where both FR_{last} and FR_{first} were mean FRs for the same given state in the flanking periods. To determine how the behavioral state regulation of FRs unfolds across the post hunt period (Figure 5E), we divided the timeline into two 24 hour bins (centered at 12hr and 36hr) and a 12 hour (centered at 60hr) final period.

FR change correlation plots (Figure 5C, D) were made by a similar method, but instead mean FRs were found for each instance of a behavioral state (NREM, REM, quiet/active wake) across the extended period (no flanking window restriction). That is, wake percent change was calculated $\%change=100*(FR_{n}- FR_{first})/ FR_{n}$, where FR_{n} was the mean FR for an instance of either active/quiet wake in the period and FR_{first} was the mean FR for the first quiet wake in that same period. Sleep percent change was calculated relative to the first NREM FR.

Spike Extraction, Clustering, and Spike Sorting

Spike extraction, clustering, and sorting were done as previously described[3,6,36,77]. Briefly, putative spikes were identified by greater than or equal to 4 standard deviations from mean signal. Using principal component analysis (PCA), the spikes from each channel were clustered using KlustaKwik[82].Clusters were classified and scored using a random forest model based on 1200 manually scored clusters encompassing 19 features (e.g. interspike interval (ISI)

contamination, waveform template matching, waveform kinetics, and noise contamination). Only single-unit clusters that were classified as high quality were used for our firing rate analyses. Clusters were further classified by their putative cell type, regular spiking (RSU) or putative fast spiking (FS), using established criteria[3,6,36,77].

Hunting Firing Rate Modulation

In order to determine which hunting behaviors significantly modulate firing rates, we took a bootstrap reshuffling approach. Firing rates were smoothed with a Gaussian kernel (σ = 3s for RSU and 5s for FS cells; chosen empirically based on FR variance during this behavior while still capturing true FR dynamics). The behavior times for a whole hunting session (10 crickets) were shifted randomly (retaining the relative behavior time intervals) within an expanded time window (+1 hour on either side). This shuffling was done 500 times for each cell. For each shuffle, the FR_{ICI}, $FR_{pursuit}$, $FR_{consumption}$, was determined for every cricket. Both $FR_{pursuit}$ and $FR_{consumption}$ were normalized to the corresponding prior FR_{ICI}. This created a shuffle control distribution, where the actual normalized $FR_{pursuit}$ and $FR_{consumption}$ when above 95th or below 5th percentile were deemed significant (upward and downward, respectively). Firing rate histograms around pursuit start and cricket capture were made by aligning a 30 second window around those times and normalizing to an 8 second baseline period at the beginning. This was done to focus on the FR dynamics specifically around those short behavioral moments.

Timepoint Analysis of Ensemble Firing Rates

To calculate firing rates at discrete timepoints, we clustered spiking data from each animal at multiple timepoints pre- and post-hunting across 6-hour bins. We then examined each putative cluster and identified high-quality clusters at each timepoint. We calculated firing rates by taking the inverse of the mean interspike interval (ISI) for each cluster to account for the variable on/off time durations for units clustered in these windows.

Continuous Single Unit Analysis

To establish the presence and persistence of continuous single units throughout our recordings, we set “on” and “off” times for each high-quality cluster during our recordings. As previously described [3,6,36] we examined each cluster’s ISI contamination, restricting “on” times to periods when a cluster’s hourly %ISIs <2.5ms was equal to or below 4%. We also calculated the hourly sum of squared error for each hourly waveform and compared to the average waveform and examined waveforms on an hourly basis to ensure waveform shape and peak amplitude

remained stable. Using this combination of metrics, we assigned “on” and “off” times for each cluster and considered only units that were online for 70% of the experiment duration.

Confocal image acquisition and analysis

Chemogenetic Disruption of V1 Quantification

CFos expression in PV-Cre^{+} and PV-Cre^{-} animals was quantified as previously described[35,36]. We created maximum projection images from z-stacks taken with a 20x objective in V1 of fixed slices from both cohorts of animals. Images were background subtracted with a rolling ball radius of 50 pixels. NeuN neurons were traced manually from the NeuN channel, and the cFos+ neurons were identified by thresholding in the cFos channel of the image. NeuN labeled and NeuN/cFos double-labeled neurons were quantified from all V1 images to find a total ratio of (NeuN+cFos+ neurons/ total NeuN+ neurons) per animal using ImageJ (NIH, Washington, DC).

Dendritic Spine Quantification

High-resolution, large-scale imaging of spine density and morphology in L2/3 pyramidal neurons was performed using an inverted confocal laser scanning microscope (LSM880, Zeiss). The localization of pyramidal neurons to V1b was first confirmed with a 10x dry objective (NA 0.45). The entire apical and basal trees of each neuron were imaged using a 63x oil objective (NA 1.4) at 1024 x 1024 pixels (pixel size of 220 x 200 x 300nm (Day 6, Day 6 + XPro) or 90 x 90 x 300nm (Day 1)). To improve resolution and signal to noise ratio, images were deconvolved in Huygens (Scientific Volume Imaging) using the classic maximum likelihood estimation (CMLE) algorithm. The entire dendritic trees and all spines were traced manually using the Filament Tracer module in Imaris (Oxford Instruments). Dendritic spine density was calculated for each dendritic segment, and densities and spine head diameters were obtained using the Statistics module in Imaris.

Representative images were improved for clarity by removing signals from other dendrites in Imaris as follows: the selected dendrite was traced as a new filament and used to reconstruct a surface with a low intensity threshold using the Surface module. This artificially enlarges the surface so that it becomes a cylinder encompassing the dendritic shaft and all the attached spines. The fluorescence signal of all pixels outside of that surface were then set to 0 and in effect masked, so that only the dendritic stretch of interest would be shown in the representative picture. Brightness and contrast were subsequently enhanced using the unsharpen filter in Photoshop (Adobe).

Statistical Analyses

Data analysis was performed using Graphpad Prism or custom code written in MATLAB (see Key Resources Table, available on GitHub). Values were reported in the text body as mean ± standard error of the mean (SEM). Individual data points represent session averages on behavioral curves, individual animals on behavioral plots, and individual neurons on firing rate plots except where noted otherwise. Parametric or non-parametric tests were chosen depending on whether data passed normality tests. To compare the means of two non-normally distributed groups, we used a Wilcoxon Rank Sum test with Bonferroni correction. To compare pairs of non-normally distributed data, we used a Wilcoxon Sign Rank test with Bonferroni correction. To compare differences within a single group across multiple timepoints, we used a Friedmann's test with Dunn correction; between two groups across multiple timepoints, we used a two-way ANOVA with Tukey-Kramer correction. Comparison of cumulative distributions was done with Kolgornov-Smirnov or Anderson-Darling tests. For determining significant firing rate modulation during hunting epochs (across epoch types and valence) across multiple sessions, a Friedman test with Tukey-Kramer post hoc (e.g. Figure 2G) or Cochran's Q (i.e. Figure S2) was used. Correlation strength and significance between firing rates and behavioral state was calculated using Pearson's *r*. To compare multiple groups to a fixed mean (usually 0), we used one-sample t-tests with Bonferroni correction. Statistical significance was considered to be $p<0.05$ and is indicated as * for $p<0.05$, ** for $p<0.01$, *** for $p<0.001$, and **** for $p<0.0001$.

RESOURCE AVAILABILITY

Lead Contact

Further information and requests for reagents and resources should be directed to and will be fulfilled by the Lead Contact, Gina Turrigiano (turrigiano@brandeis.edu).

Materials Availability

This study did not generate new reagents.

Data and Code Availability

Processed data that went into generating figures will be deposited in a publicly available database such as Figshare upon acceptance. Large unprocessed datasets will be made available upon request. All code will be deposited at Github upon acceptance.

ACKNOWLEDGEMENTS

We thank members of the Turrigiano lab for many helpful discussions, Lirong Wang and Zhe Meng for help with animal colony maintenance, the Brandeis Light Microscopy Core Facility, and the Brandeis Machine Shop for their assistance. XPRO1595 was a gift from INmuneBio (Boca Raton, FL, USA). Funding provided by T32NS007292 (BJL, NFW, MRS), R01 EY025613 (GGT), R35NS111562 (GGT), and Simons Foundation grant 901199 (GGT).

AUTHOR CONTRIBUTIONS

Conceptualization: D.P.L, B.J.L., G.G.T.; Methodology: D.P.L., B.J.L., B.A.C., D.B., G.G.T.; Software: D.P.L., B.A.C., B.J.L., M.R.S., N.F.W.; Formal Analysis: D.P.L., B.A.C., D.B., M.R.S., N.F.W., K.B.B.; Investigation: D.P.L, D.B., B.J.L., M.R.S., N.F.W., K.B.B.; Writing: D.P.L., B.A.C., G.G.T.; Visualization: D.P.L., B.A.C., D.B., M.R.S., N.F.W.; Data Curation: D.P.L., D.B.; Supervision: G.G.T.; Funding Acquisition: G.G.T.

DECLARATION OF INTERESTS

The authors declare no competing interests.

REFERENCES

1. Turrigiano, G. G. & Nelson, S. B. Homeostatic plasticity in the developing nervous system. *Nat. Rev. Neurosci.* **5**, 97–107 (2004).
2. Abbott, L. F. & Nelson, S. B. Synaptic plasticity: taming the beast. *Nat. Neurosci.* **3**, 1178–1183 (2000).
3. Hengen, K. B., Torrado Pacheco, A., McGregor, J. N., Van Hooser, S. D. & Turrigiano, G. G. Neuronal Firing Rate Homeostasis Is Inhibited by Sleep and Promoted by Wake. *Cell* **165**, 180–191 (2016).
4. Hengen, K. B., Lambo, M. E., Van Hooser, S. D., Katz, D. B. & Turrigiano, G. G. Firing Rate Homeostasis in Visual Cortex of Freely Behaving Rodents. *Neuron* **80**, 335–342 (2013).
5. Keck, T. *et al.* Synaptic Scaling and Homeostatic Plasticity in the Mouse Visual Cortex In Vivo. *Neuron* **80**, 327–334 (2013).

6. Torrado Pacheco, A., Bottorff, J., Gao, Y. & Turrigiano, G. G. Sleep Promotes Downward Firing Rate Homeostasis. *Neuron* **109**, 530-544.e6 (2021).
7. Barnes, S. J. *et al.* Subnetwork-Specific Homeostatic Plasticity in Mouse Visual Cortex In Vivo. *Neuron* **86**, 1290–1303 (2015).
8. Wu, Y. K., Hengen, K. B., Turrigiano, G. G. & Gjorgjieva, J. Homeostatic mechanisms regulate distinct aspects of cortical circuit dynamics. *Proc. Natl. Acad. Sci.* **117**, 24514–24525 (2020).
9. McGregor, J. N. *et al.* Failure in a population: Tauopathy disrupts homeostatic set-points in emergent dynamics despite stability in the constituent neurons. *Neuron* **112**, 3567-3584.e5 (2024).
10. Dhawale, A. K. *et al.* Automated long-term recording and analysis of neural activity in behaving animals. *eLife* **6**, e27702 (2017).
11. Jensen, K. T., Kadmon Harpaz, N., Dhawale, A. K., Wolff, S. B. E. & Ölveczky, B. P. Long-term stability of single neuron activity in the motor system. *Nat. Neurosci.* **25**, 1664–1674 (2022).
12. Landry, Stuart O. The Rodentia as Omnivores. *Q. Rev. Biol.* **45**, 351–372 (1970).
13. Clark, D. A. Foraging Behavior of a Vertebrate Omnivore (Rattus Rattus): Meal Structure, Sampling, and Diet Breadth. *Ecology* **63**, 763–772 (1982).
14. Polsky, R. H. Influence of eating dead prey on subsequent capture of live prey in golden hamsters. *Physiol. Behav.* **20**, 677–680 (1978).
15. Dean, P. & Redgrave, P. The superior colliculus and visual neglect in rat and hamster. I. behavioural evidence. *Brain Res. Rev.* **8**, 129–141 (1984).
16. Langley, W. M. Grasshopper mouse's use of visual cues during a predatory attack. *Behav. Processes* **19**, 115–125 (1989).
17. Hoy, J. L., Yavorska, I., Wehr, M. & Niell, C. M. Vision Drives Accurate Approach Behavior during Prey Capture in Laboratory Mice. *Curr. Biol.* **26**, 3046–3052 (2016).

18. Hoy, J. L., Bishop, H. I. & Niell, C. M. Defined Cell Types in Superior Colliculus Make Distinct Contributions to Prey Capture Behavior in the Mouse. *Curr. Biol.* **29**, 4130-4138.e5 (2019).
19. Zhao, Z. *et al.* Zona incerta GABAergic neurons integrate prey-related sensory signals and induce an appetitive drive to promote hunting. *Nat. Neurosci.* **22**, 921–932 (2019).
20. Michaiel, A. M., Abe, E. T. & Niell, C. M. Dynamics of gaze control during prey capture in freely moving mice. *eLife* **9**, e57458 (2020).
21. Groves Kuhnle, C., Grimes, M., Casanova, V. M. S., Turrigiano, G. G. & Hooser, S. D. V. Juvenile Shank3 KO Mice Adopt Distinct Hunting Strategies during Prey Capture Learning. *eNeuro* **9**, (2022).
22. Galvin, L., Mirza Agha, B., Saleh, M., Mohajerani, M. H. & Whishaw, I. Q. Learning to cricket hunt by the laboratory mouse (*Mus musculus*): Skilled movements of the hands and mouth in cricket capture and consumption. *Behav. Brain Res.* **412**, 113404 (2021).
23. Bissen, D. *et al.* Prey capture learning drives critical period-specific plasticity in mouse binocular visual cortex. 2025.01.28.635373 Preprint at https://doi.org/10.1101/2025.01.28.635373 (2025).
24. Johnson, K. P. *et al.* Cell-type-specific binocular vision guides predation in mice. *Neuron* **109**, 1527-1539.e4 (2021).
25. Holmgren, C. D. *et al.* Visual pursuit behavior in mice maintains the pursued prey on the retinal region with least optic flow. *eLife* **10**, e70838 (2021).
26. Barnes, S. J., Keller, G. B. & Keck, T. Homeostatic regulation through strengthening of neuronal network-correlated synaptic inputs. *eLife* **11**, e81958 (2022).
27. Barnes, S. J. *et al.* Deprivation-Induced Homeostatic Spine Scaling *In Vivo* Is Localized to Dendritic Branches that Have Undergone Recent Spine Loss. *Neuron* **96**, 871-882.e5 (2017).

28. Kaneko, M., Stellwagen, D., Malenka, R. C. & Stryker, M. P. Tumor Necrosis Factor-α Mediates One Component of Competitive, Experience-Dependent Plasticity in Developing Visual Cortex. *Neuron* **58**, 673–680 (2008).
29. Mrsic-Flogel, T. D. *et al.* Homeostatic Regulation of Eye-Specific Responses in Visual Cortex during Ocular Dominance Plasticity. *Neuron* **54**, 961–972 (2007).
30. Pozo, K. & Goda, Y. Unraveling Mechanisms of Homeostatic Synaptic Plasticity. *Neuron* **66**, 337–351 (2010).
31. Stellwagen, D. & Malenka, R. C. Synaptic scaling mediated by glial TNF-α. *Nature* **440**, 1054–1059 (2006).
32. Turrigiano, G. Homeostatic Synaptic Plasticity: Local and Global Mechanisms for Stabilizing Neuronal Function. *Cold Spring Harb. Perspect. Biol.* **4**, a005736 (2012).
33. Procacci, N. M. *et al.* Context-dependent modulation of natural approach behaviour in mice. *Proc. R. Soc. B Biol. Sci.* **287**, 20201189 (2020).
34. Yu, J. Y. *et al.* Knock-in rats expressing Cre and Flp recombinases at the Parvalbumin locus. *bioRxiv* 386474 (2018) doi:10.1101/386474.
35. Wen, W. & Turrigiano, G. G. Developmental Regulation of Homeostatic Plasticity in Mouse Primary Visual Cortex. *J. Neurosci.* **41**, 9891–9905 (2021).
36. Bottorff, J., Padgett, S. & Turrigiano, G. G. Basal forebrain cholinergic activity is necessary for upward firing rate homeostasis in the rodent visual cortex. *Proc. Natl. Acad. Sci.* **121**, e2317987121 (2024).
37. Chattopadhyaya, B. *et al.* Experience and Activity-Dependent Maturation of Perisomatic GABAergic Innervation in Primary Visual Cortex during a Postnatal Critical Period. *J. Neurosci.* **24**, 9598–9611 (2004).
38. Nahmani, M. & Turrigiano, G. G. Deprivation-Induced Strengthening of Presynaptic and Postsynaptic Inhibitory Transmission in Layer 4 of Visual Cortex during the Critical Period. *J. Neurosci.* **34**, 2571–2582 (2014).

39. Lambo, M. E. & Turrigiano, G. G. Synaptic and Intrinsic Homeostatic Mechanisms Cooperate to Increase L2/3 Pyramidal Neuron Excitability during a Late Phase of Critical Period Plasticity. *J. Neurosci.* **33**, 8810–8819 (2013).
40. Maffei, A. & Turrigiano, G. G. Multiple Modes of Network Homeostasis in Visual Cortical Layer 2/3. *J. Neurosci.* **28**, 4377–4384 (2008).
41. Keck, T. *et al.* Loss of Sensory Input Causes Rapid Structural Changes of Inhibitory Neurons in Adult Mouse Visual Cortex. *Neuron* **71**, 869–882 (2011).
42. Gainey, M. A. & Feldman, D. E. Multiple shared mechanisms for homeostatic plasticity in rodent somatosensory and visual cortex. *Philos. Trans. R. Soc. B Biol. Sci.* **372**, 20160157 (2017).
43. Niell, C. M. & Stryker, M. P. Highly Selective Receptive Fields in Mouse Visual Cortex. *J. Neurosci.* **28**, 7520–7536 (2008).
44. Cardin, J. A., Palmer, L. A. & Contreras, D. Stimulus Feature Selectivity in Excitatory and Inhibitory Neurons in Primary Visual Cortex. *J. Neurosci.* **27**, 10333–10344 (2007).
45. Cary, B. A. & Turrigiano, G. G. Stability of neocortical synapses across sleep and wake states during the critical period in rats. *eLife* **10**, e66304 (2021).
46. Miyawaki, H. & Diba, K. Regulation of Hippocampal Firing by Network Oscillations during Sleep. *Curr. Biol.* **26**, 893–902 (2016).
47. Turrigiano, G. G., Leslie, K. R., Desai, N. S., Rutherford, L. C. & Nelson, S. B. Activity-dependent scaling of quantal amplitude in neocortical neurons. *Nature* **391**, 892–896 (1998).
48. Wierenga, C. J., Walsh, M. F. & Turrigiano, G. G. Temporal Regulation of the Expression Locus of Homeostatic Plasticity. *J. Neurophysiol.* **96**, 2127–2133 (2006).
49. Steinmetz, C. C. & Turrigiano, G. G. Tumor Necrosis Factor-α Signaling Maintains the Ability of Cortical Synapses to Express Synaptic Scaling. *J. Neurosci.* **30**, 14685–14690 (2010).

50. Smilovic, D., Rietsche, M., Drakew, A., Vuksic, M. & Deller, T. Constitutive tumor necrosis factor (TNF)-deficiency causes a reduction in spine density in mouse dentate granule cells accompanied by homeostatic adaptations of spine head size. *J. Comp. Neurol.* **530**, 656–669 (2022).
51. Wen, W., Prada, A. M. & Turrigiano, G. G. Modular Arrangement of Synaptic and Intrinsic Homeostatic Plasticity within Visual Cortical Circuits. 2024.06.01.596982 Preprint at https://doi.org/10.1101/2024.06.01.596982 (2025).
52. Keck, T. *et al.* Massive restructuring of neuronal circuits during functional reorganization of adult visual cortex. *Nat. Neurosci.* **11**, 1162–1167 (2008).
53. Ma, Z., Turrigiano, G. G., Wessel, R. & Hengen, K. B. Cortical Circuit Dynamics Are Homeostatically Tuned to Criticality *In Vivo*. *Neuron* **104**, 655-664.e4 (2019).
54. Slomowitz, E. *et al.* Interplay between population firing stability and single neuron dynamics in hippocampal networks. *eLife* **4**, e04378 (2015).
55. Ruggiero, A. *et al.* NMDA receptors regulate the firing rate set point of hippocampal circuits without altering single-cell dynamics. *Neuron* **113**, 244-259.e7 (2025).
56. Styr, B. *et al.* Mitochondrial Regulation of the Hippocampal Firing Rate Set Point and Seizure Susceptibility. *Neuron* **102**, 1009-1024.e8 (2019).
57. Mizuseki, K. & Buzsáki, G. Preconfigured, Skewed Distribution of Firing Rates in the Hippocampus and Entorhinal Cortex. *Cell Rep.* **4**, 1010–1021 (2013).
58. Keck, T. *et al.* Integrating Hebbian and homeostatic plasticity: the current state of the field and future research directions. *Philos. Trans. R. Soc. B Biol. Sci.* **372**, 20160158 (2017).
59. Kleidonas, D. *et al.* Microglia modulate TNFα-mediated synaptic plasticity. *Glia* **71**, 2117–2136 (2023).
60. Desai, N. S., Rutherford, L. C. & Turrigiano, G. G. Plasticity in the intrinsic excitability of cortical pyramidal neurons. *Nat. Neurosci.* **2**, 515–520 (1999).

61. Desai, N. S., Cudmore, R. H., Nelson, S. B. & Turrigiano, G. G. Critical periods for experience-dependent synaptic scaling in visual cortex. *Nat. Neurosci.* **5**, 783–789 (2002).

62. Aton, S. J., Suresh, A., Broussard, C. & Frank, M. G. Sleep Promotes Cortical Response Potentiation Following Visual Experience. *Sleep* **37**, 1163–1170 (2014).

63. Aton, S. J. *et al.* Mechanisms of Sleep-Dependent Consolidation of Cortical Plasticity. *Neuron* **61**, 454–466 (2009).

64. Dumoulin Bridi, M. C. *et al.* Rapid eye movement sleep promotes cortical plasticity in the developing brain. *Sci. Adv.* **1**, e1500105 (2015).

65. Frank, M. G. Sleep and plasticity in the visual cortex: more than meets the eye. *Curr. Opin. Neurobiol.* **44**, 8–12 (2017).

66. Diba, K. & Buzsáki, G. Forward and reverse hippocampal place-cell sequences during ripples. *Nat. Neurosci.* **10**, 1241–1242 (2007).

67. Frank, M. G., Issa, N. P. & Stryker, M. P. Sleep Enhances Plasticity in the Developing Visual Cortex. *Neuron* **30**, 275–287 (2001).

68. Ji, D. & Wilson, M. A. Coordinated memory replay in the visual cortex and hippocampus during sleep. *Nat. Neurosci.* **10**, 100–107 (2007).

69. Josselyn, S. A. & Tonegawa, S. Memory engrams: Recalling the past and imagining the future. *Science* **367**, eaaw4325 (2020).

70. Lee, A. K. & Wilson, M. A. Memory of Sequential Experience in the Hippocampus during Slow Wave Sleep. *Neuron* **36**, 1183–1194 (2002).

71. Wilson, M. A. & McNaughton, B. L. Reactivation of Hippocampal Ensemble Memories During Sleep. *Science* **265**, 676–679 (1994).

72. Carr, M. F., Jadhav, S. P. & Frank, L. M. Hippocampal replay in the awake state: a potential substrate for memory consolidation and retrieval. *Nat. Neurosci.* **14**, 147–153 (2011).

73. Jadhav, S. P., Kemere, C., German, P. W. & Frank, L. M. Awake Hippocampal Sharp-Wave Ripples Support Spatial Memory. *Science* **336**, 1454–1458 (2012).

74. Tang, W., Shin, J. D., Frank, L. M. & Jadhav, S. P. Hippocampal-Prefrontal Reactivation during Learning Is Stronger in Awake Compared with Sleep States. *J. Neurosci.* **37**, 11789–11805 (2017).

75. Shin, J. D., Tang, W. & Jadhav, S. P. Dynamics of Awake Hippocampal-Prefrontal Replay for Spatial Learning and Memory-Guided Decision Making. *Neuron* **104**, 1110-1125.e7 (2019).

76. Wu, C.-H., Ramos, R., Katz, D. B. & Turrigiano, G. G. Homeostatic synaptic scaling establishes the specificity of an associative memory. *Curr. Biol.* **31**, 2274-2285.e5 (2021).

77. Torrado Pacheco, A. *et al.* Rapid and active stabilization of visual cortical firing rates across light–dark transitions. *Proc. Natl. Acad. Sci.* **116**, 18068–18077 (2019).

78. Zalevsky, J. *et al.* Dominant-Negative Inhibitors of Soluble TNF Attenuate Experimental Arthritis without Suppressing Innate Immunity to Infection. *J. Immunol.* **179**, 1872–1883 (2007).

79. Barnum, C. J. *et al.* Peripheral Administration of the Selective Inhibitor of Soluble Tumor Necrosis Factor (TNF) XPro®1595 Attenuates Nigral Cell Loss and Glial Activation in 6-OHDA Hemiparkinsonian Rats. *J. Park. Dis.* **4**, 349–360 (2014).

80. Mathis, A. *et al.* DeepLabCut: markerless pose estimation of user-defined body parts with deep learning. *Nat. Neurosci.* **21**, 1281–1289 (2018).

81. Nath, T. *et al.* Using DeepLabCut for 3D markerless pose estimation across species and behaviors. *Nat. Protoc.* **14**, 2152–2176 (2019).

82. Harris, K. D., Henze, D. A., Csicsvari, J., Hirase, H. & Buzsáki, G. Accuracy of Tetrode Spike Separation as Determined by Simultaneous Intracellular and Extracellular Measurements. *J. Neurophysiol.* **84**, 401–414 (2000).

Figure 1. Rapid, V1-dependent prey capture learning in juvenile rats

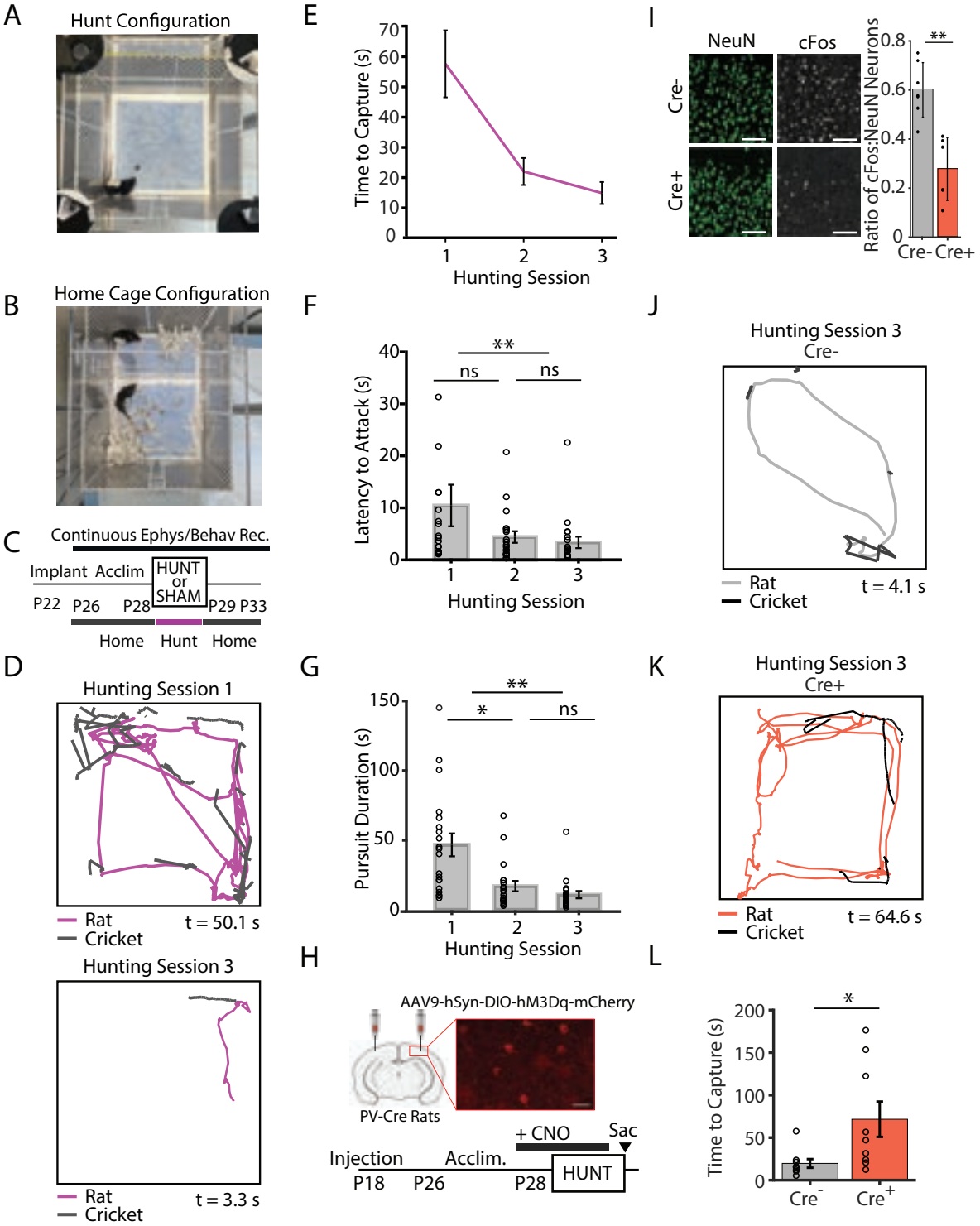

A. Prey capture learning arena in “hunting” configuration with rat and cricket.

B. Prey capture learning arena in “home cage” configuration with rat, bedding, food, water, and littermate in adjacent chamber for social interaction.

C. Experimental timeline for chronic behavior and electrophysiology recordings for prey capture learning.

D. Example trajectories of rat and cricket during one hunt by naïve (hunting session 1) or experienced (hunting session 3) rat. Magenta: rat position, black: cricket position; discontinuities due to cricket jumps. Time to capture is signified by t (seconds).

E-G. (E) Average time to capture, (F) latency to attack, and (G) pursuit durations for electrode-implanted rats for hunting sessions 1-3. Circles represent individual animal averages per session (n=20 rats, 10 hunts/session) error bars represent the mean +/- SEM. Friedmann Test with Dunn Correction, Time to capture: HS1-HS2: $p=0.003$, HS1-HS3: $p<0.0001$, HS2-HS3: $p=0.5$; Latency to Attack: HS1-HS2: $p=0.05$, HS1-HS3: $p=0.003$, HS2-HS3: $p>0.9$; Pursuit Duration: HS1-HS2: $p=0.006$, HS1-HS3: $p<0.0001$, HS2-HS3: $p=0.4$.

H. Experimental timeline for DREADDs-mediated chemogenetic inhibition of V1 during prey capture learning. Inset: PV interneurons expressing excitatory DREADDs (labeled with mCherry). Scale bar=50μm.

I. Fraction of NeuN+ pyramidal neurons that are also cFos+, in littermates with (Cre+) or without (Cre-) excitatory DREADDs expressed in PV neurons. Wilcoxon Rank Sum test, $p=0.001$. PV-Cre-: n=7 rats, cFos: n=1955 neurons, NeuN: n=3332 neurons; PV-Cre+, n=6 rats, cFos: n=855 neurons, NeuN: n=2996 neurons.

J, K. Example trajectories of rat and cricket from hunting session 3 for (J) Cre- and (K) Cre+ animal in presence of CNO.

L. Average time to capture averaged across all 3 hunting sessions for each animal on D1, for PV-Cre- vs PV-Cre+ rats (Cre-: n=9 animals; Cre+: n=9 animals), Wilcoxon Rank Sum test, $p=0.01$. Here and onward, all error bars represent the mean +/- SEM unless otherwise indicated.

Figure 2. The activity of V1b neurons becomes tuned to behavior during prey capture learning

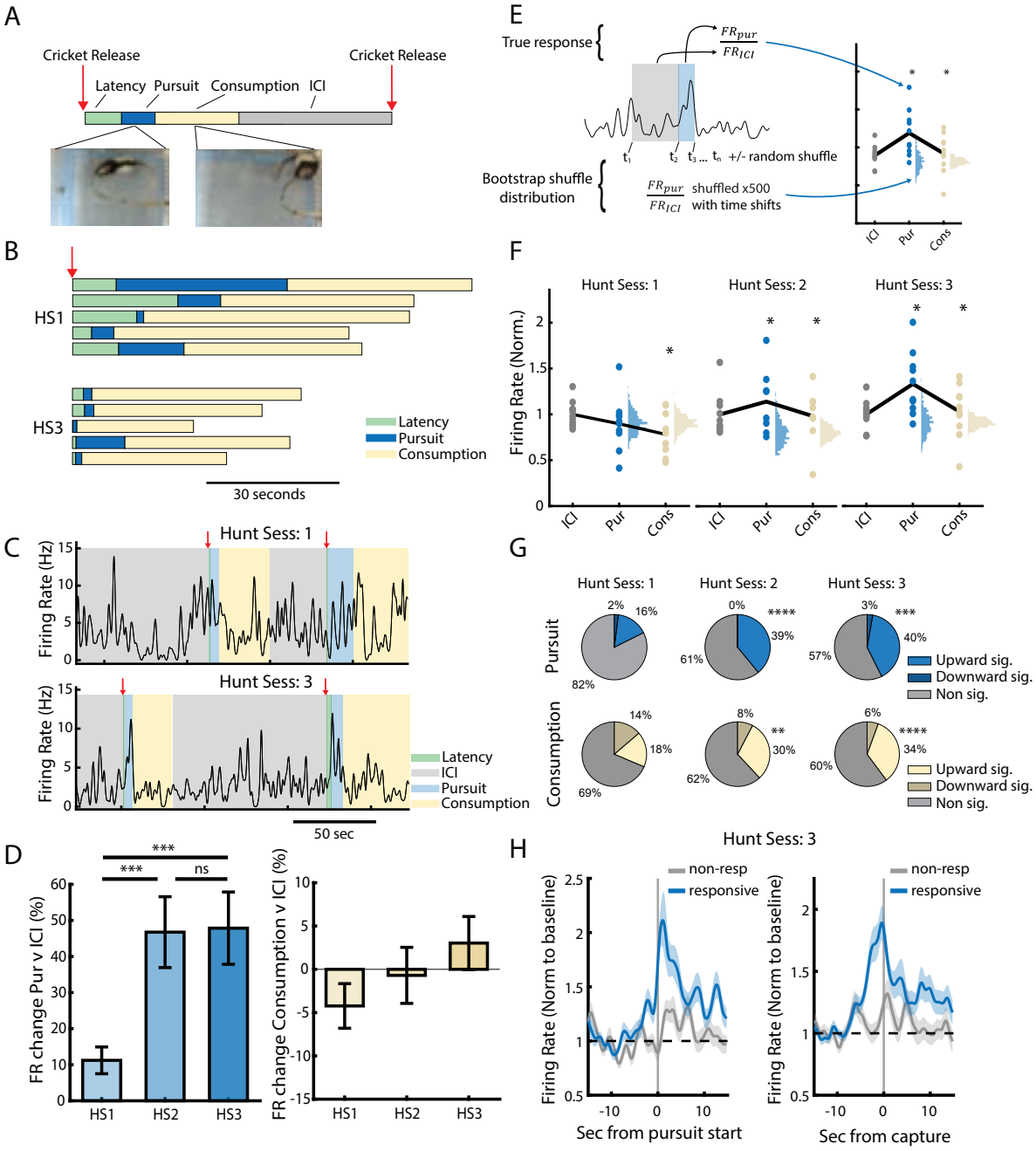

A. Example ethogram showing behavioral sequence during a hunt. ICI = inter-cricket interval.

B. 5 example ethograms from the first (HS1) and third (HS3) hunting session, illustrating variability in timing.

C. Two example firing rate (FR) traces from the same cell on HS1 and HS3, respectively. Behavioral sequence labels indicated with colored boxes.

D. Percentage change in FR from ICI during pursuit (left) and consumption (right) across hunting sessions. Repeated measures ANOVA with Tukey-Kramer post hoc: Pursuit: HS1-HS2: $p=0.0006$, HS1-HS3: $p=0.0009$, HS2-HS3: $p>0.9$. Consumption: HS1-HS2: $p=0.7$, HS1-HS3: $p=0.2$, HS2-HS3: $p=0.5$.

E. Schematic showing bootstrap approach to determining significant FR modulation during hunting behaviors.

F. Illustration of bootstrap results showing a single cell's responses across the 3 hunting sessions. Circles indicate actual normalized FRs during given behavior. Sideways histograms represent calculated bootstrap shuffle distributions. Asterisks indicate bootstrap significance ($<5^{th}$ or $>95^{th}$ percentiles).

G. Percentage breakdown of up/down/non-significant modulation of the RSUs across prey capture learning. Friedman Test with Tukey-Kramer post hoc; Pursuit (top row): HS1-HS2: $p=0.0001$, HS1-HS3: $p=0.0002$. Consumption (bottom row): HS1-HS2: $p=0.0009$, HS1-HS3: $p=0.0002$.

H. Normalized FRs aligned to either pursuit initiation (left) or capture (right) for responsive and non-responsive RSUs. Data from hunting session 3 only. FRs are normalized to an 8 second window preceding pursuit initiation or capture events.

Figure 3. Prey capture learning induces a slowly developing and persistent increase in V1b firing rates

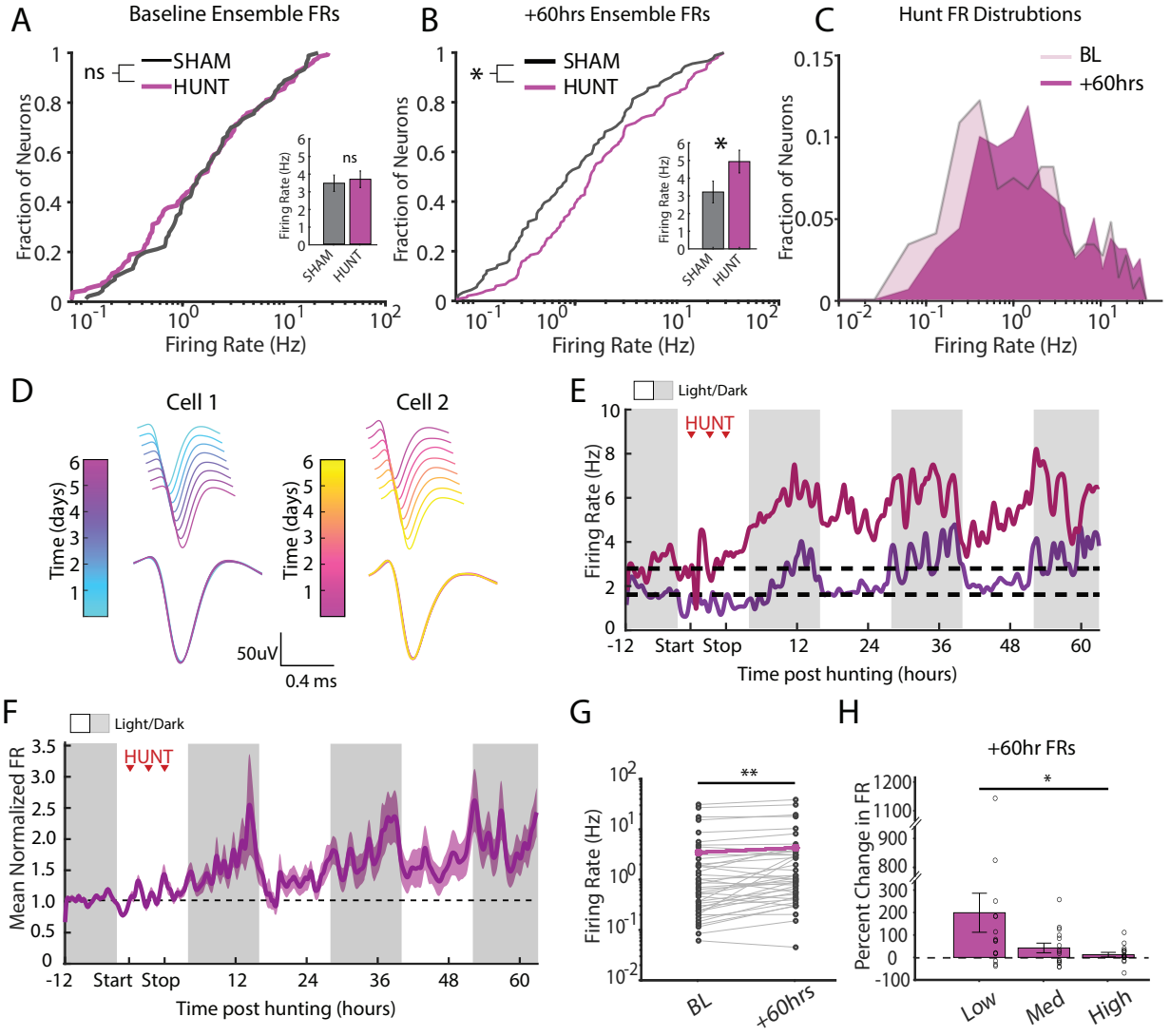

A. Distributions of ensemble FRs for Sham (grey) and Hunt (magenta) conditions at baseline. SHAM: n=109 neurons, Hunt: n=140 neurons. Anderson Darling test, p=0.2. Inset: Average ensemble firing rates. Wilcoxon Rank Sum, p=0.09.

B. Distributions of ensemble FRs for Sham (grey) and Hunt (magenta) conditions following prey capture learning or sham. SHAM: n=91 neurons, Hunt: n=152 neurons, Anderson Darling test, p=0.01, Inset: Average ensemble firing rates. Wilcoxon Rank Sum, p=0.01.

C. Distribution of firing rates from the hunt condition comparing baseline (BL) and 60 hours post-learning (+60hrs).

D. Average waveform traces for two example RSUs recorded from the same electrode. Each spike waveform was color-coded by day to illustrate stability; the overlay across days is shown below.

E. FRs of two individual RSUs (red and purple) measured continuously for 12 hours prior to and 62 hours after prey capture learning. Red arrows here and onward indicate individual hunting sessions; white/grey bars indicate light/dark periods.

F. Mean, normalized FRs of all continuously recorded RSUs (n=45 from 6 animals). Here and onward, shaded area around mean firing rate indicates SEM.

G. Average FRs for all continuously recorded RSUs in Figure 3F, measured at baseline and 60 hours post-prey capture learning. Wilcoxon Sign Rank test, p=0.003. Purple line indicates mean firing rates (baseline: 2.9Hz, 60hrs: 3.6Hz).

H. Percent change in RSU firing rates 60 hours post-hunting, grouped into tertiles (low, medium, high) based on baseline firing rates. One-way ANOVA, p=0.04.

Figure 4. FSU firing rates are persistently increased by prey capture learning

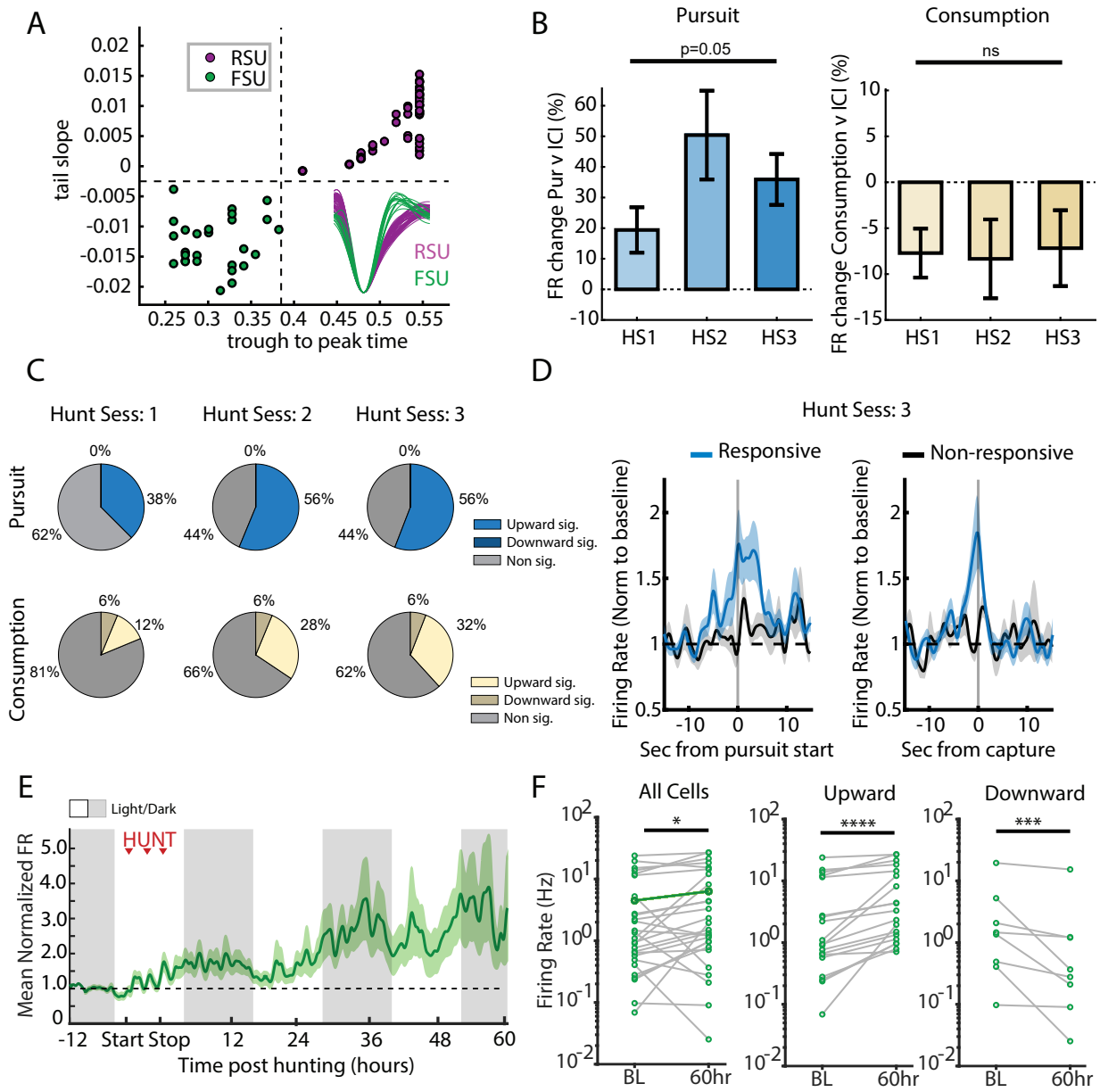

A. Plot of spike trough-to-peak vs. tail slope showing segregation into FSUs (green) and RSUs (magenta).

B. Percentage change in FR during pursuit (left) and consumption (right) across hunting sessions. Repeated measures ANOVA with Tukey-Kramer post hoc test, Pursuit: $p=0.05$, Consumption $p=0.8$.

C. Pie charts indicating percentage breakdown of up/down/non-significant modulation of FSUs, determined by bootstrap analysis as in Figure 2G. Friedman test with Tukey-Kramer post hoc correction, Pursuit (top row): HS1-HS2: $p=0.2$, HS1-HS3: $p=0.09$. Consumption (bottom row): HS1-HS2: $p=0.5$, HS1-HS3: $p=0.5$.

D. Normalized FRs aligned to either pursuit start (left) or capture (right) for responsive and non-responsive FSUs.

E. Mean, normalized FR of continuously recorded FSUs (n=28 from 6 animals).

F. Left: mean FRs of individual FSUs measured at baseline (BL) and 60 hours post-prey capture learning (+60hr). Wilcoxon Sign Rank test, $p=0.01$. Middle: same, for FSUs with increased firing (n=20), Wilcoxon Sign Rank test, $p<0.0001$. Right: same, for FSUs with decreased firing (n=8), Wilcoxon Sign Rank test, $p=0.008$.

Figure 5. Learning-induced firing rate plasticity is gated by sleep/wake states

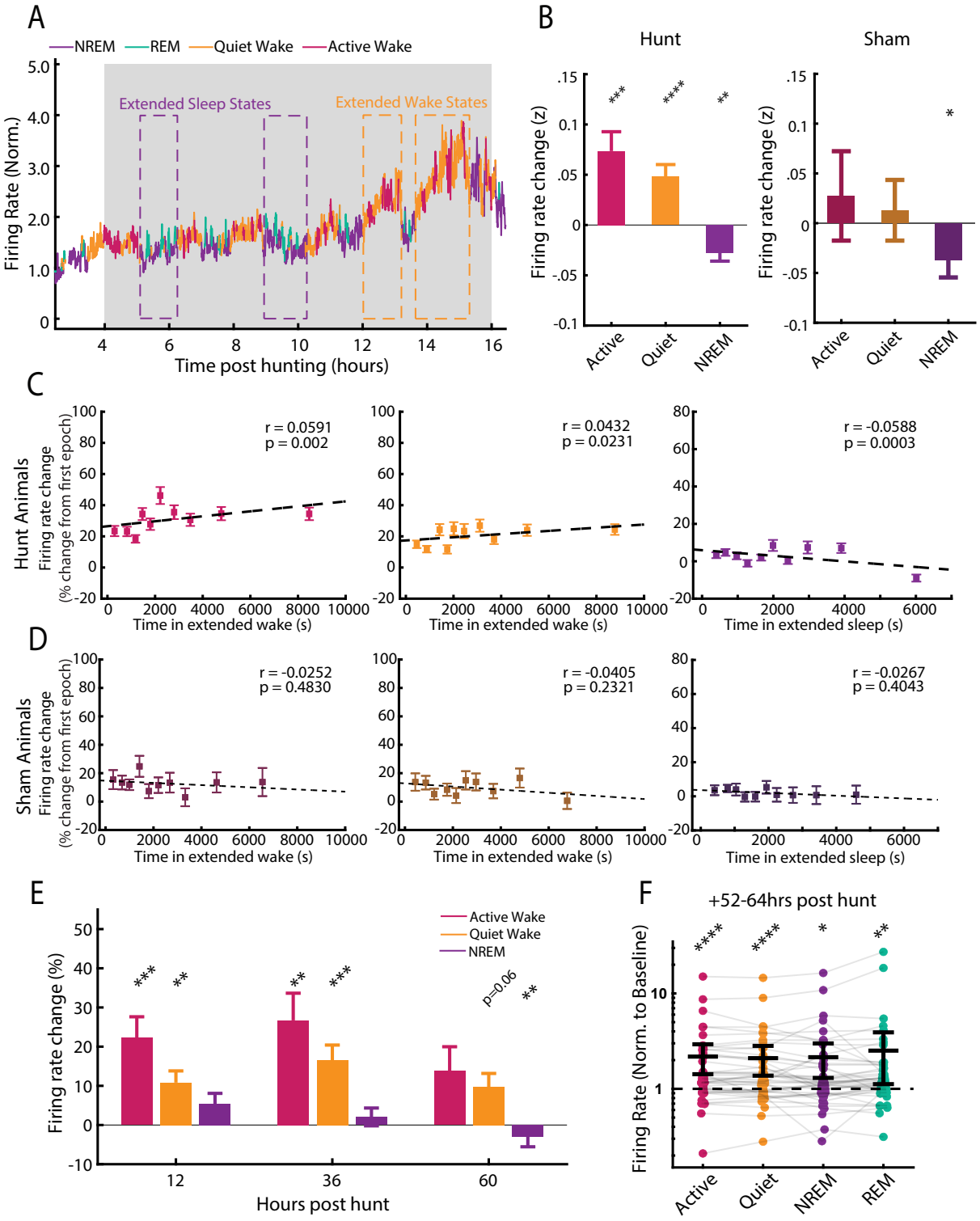

A. Ensemble average FR from one rat after hunting, color-coded by behavioral state. Two examples each of extended sleep and wake periods are highlighted.

B. Mean change in z-scored FR across all extended quite wake, active wake, and NREM episodes after hunting (left) or sham (right). One-sided Wilcoxon Sign Rank test with Bonferroni Correction p-values for Hunt condition (left): AW p=0.0006, QW p<0.0001, NREM p=0.0003. Sham (right): AW p>0.9, QW p>0.9, NREM p=0.045. Hunt: n=98 wake episodes; n=118 sleep episodes. Sham: n=60 wake episodes; n=52 sleep episodes.

C. Correlation between percentage change in FR in active wake (left), quiet wake (middle), and NREM (right) and time from start of extended wake/sleep episodes, respectively. Change is calculated from FR in the first quiet wake epoch for wake episodes and from the first NREM epoch for sleep. Scatter data points are grouped into 10 equal sized groups with means +/- SEM for visualization. Pearson r and p values were computed on the ungrouped data: AW p=0.002, QW p=0.02, NREM p=0.0003. n=2761 QW data points, 2688 AW data points, 3861 NREM data points.

D. Same as in (C) but for Sham animals. Pearson results: AW p=0.5, QW p=0.2, NREM p=0.4. n=871 QW data points, 772 AW data points, 975 NREM data points.

E. FR change across extended wake/sleep episodes measured within Active/Quiet wake and NREM states in hunt animals. Sign rank test with Bonferroni corrected p-values: 12hr AW p=0.0001, QW p=0.003, NREM p>0.9; 36hr AW p=0.001, QW p=0.0003, NREM p=0.2; 60hr AW p=0.6, QW p=0.06, NREM p=0.003.

F. Individual mean RSU firing rates post-hunt for each state, normalized to within-state firing rates in the baseline period. Sign rank test with Bonferroni corrected p-values: AW p=0.0004, QW p=0.001, NREM p=0.01, REM p=0.002. n=45 cells, 6 animals.

Figure 6. Prey capture learning has only minor effects on excitatory quantal currents and intrinsic excitability of L2/3 pyramidal neurons.

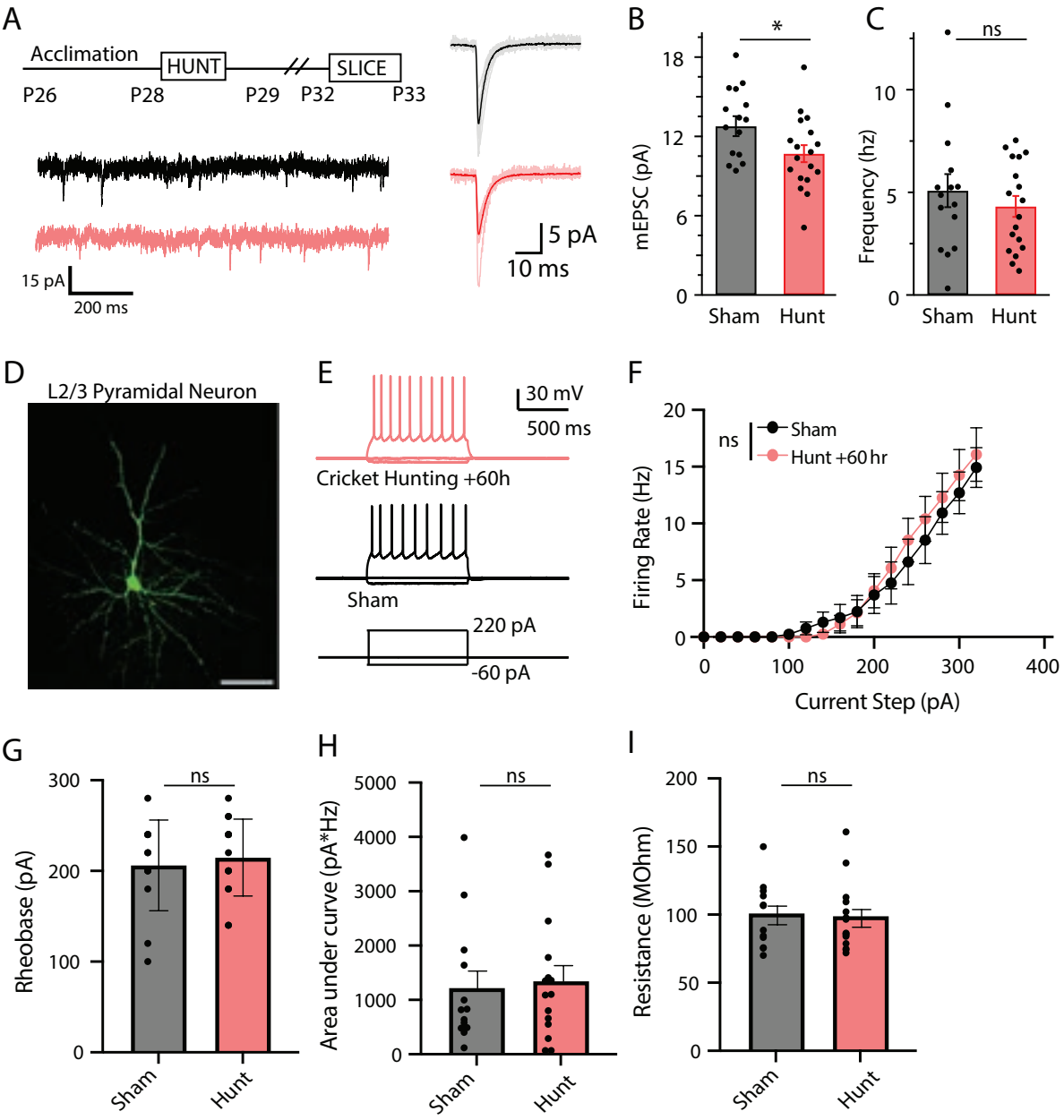

A. Top: Experimental paradigm for *ex vivo* slice electrophysiology experiments. Example mEPSC recordings (bottom) and average waveforms (right) from an individual neuron from Sham (black) and Hunt (red) conditions.

B, C. Average mEPSC amplitude (B) and frequency (C) for Sham (grey) and Hunt (red) condition. Sham: 15 neurons from 5 animals. Hunting: 18 neurons from 5 animals. Wilcoxon Rank Sum test, p=0.01 for amplitude, p=0.7 for frequency.

D. Biocytin-labeled cell fill of layer 2/3 V1b pyramidal neuron recorded from Hunt condition, scale bar = 50μm.

E. Example whole cell current clamp recordings from Sham (black) and Hunt (red) neurons in response to hyper- or depolarizing current injections.

F. Frequency vs. Current (F-I) curve for Sham (black) and Hunt (red) conditions. Here and below (G-I), Sham: 13 neurons from 5 animals; Hunting: 15 neurons from 5 animals. Repeated Measures two-way ANOVA, p=0.8.

G. Rheobase for Sham (grey) and Hunt (red) condition. Wilcoxon Rank Sum test, p=0.7.

H. Area under F-I curve (AUC) for Sham (grey) and Hunt (red) condition. Wilcoxon Rank Sum test, p=0.7.

I. Input resistance for Sham (grey) and Hunt (red) condition. Wilcoxon Rank Sum test, p=0.7.

Figure 7. Learning drives a TNFα-dependent increase in L2/3 excitatory synapse that is necessary for hunting skill retention

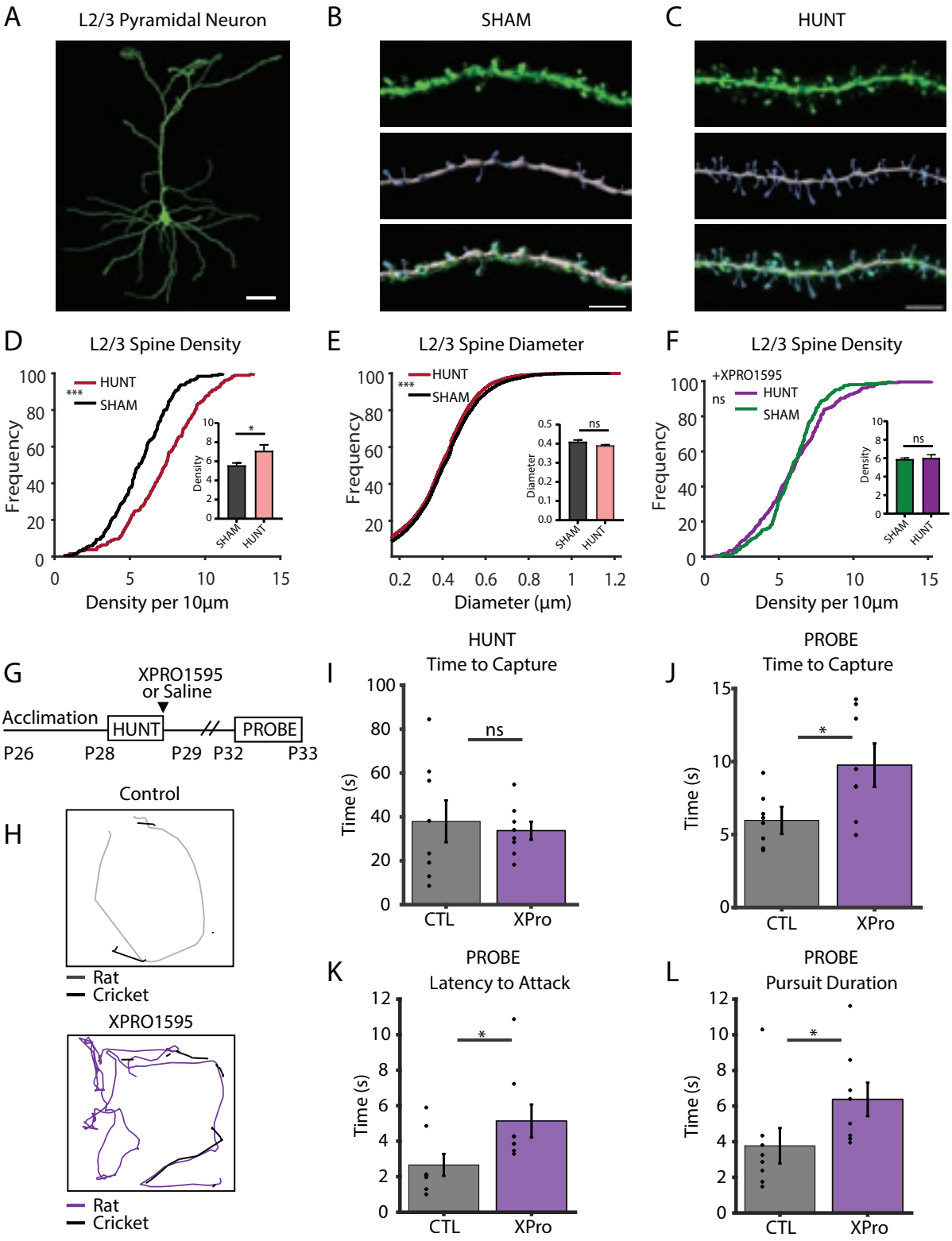

A. Example YFP-labeled mouse layer 2/3 V1b pyramidal neuron; scale bar = 50μm.

B. Top: YFP-labeled dendritic segment from Sham condition; Middle: reconstruction of dendrites (grey) and spines (blue); Bottom: Overlay of top and middle images; scale bar = 5μm.

C. Top: YFP-labeled dendritic segment from Hunt condition; Middle: reconstruction of dendrites (grey) and spines (blue); Bottom: Overlay of top and middle images. Scale bar = 5μm.

D. Cumulative distribution of L2/3 spine density across all dendritic segments, measured 3 hours after learning was complete. Sham: n=191 dendritic segments, Hunt: 189 dendritic segments, from 6 neurons and 3 animals per condition. Kolmogorov-Smirnov test, $p<0.0001$. Inset shows mean density by neuron; Unpaired t-test, $p=0.046$.

E. Cumulative distribution of L2/3 spine head diameter at same time point. Sham: n=5730 spines, Hunt: n=6831 spines, from 6 neurons and 3 animals per condition. Kolmogorov-Smirnov test, $p<0.0001$. Inset shows mean spine head diameter by neuron; Unpaired t-test, $p=0.06$.

F. Cumulative distribution of L2/3 spine density in the XPro condition, measured as above. Sham: n=208 dendritic segments, Hunt: n=259 dendritic segments, from 6 neurons and 3 animals per condition. Kolmogorov-Smirnov test, $p=0.1$. Inset shows mean density by neuron; Unpaired t-test, $p=0.8$.

G. Experimental paradigm for determining the impact of XPRO1595 on retention of hunting skills; XPRO1595 was administered 1 hour following the completion of learning on Day 1, and behavior was subsequently measured in a probe session 3 days later.

H. Top: Representative trajectory of control rat and cricket positions during probe sessions (grey: rat position, black: cricket position). Bottom: Representative trajectory of XPRO1595-injected rat and cricket positions during probe session (purple: rat position, black: cricket position).

I. Average time to capture (s) on Day 1 for control (grey) and XPRO1595-injected (purple) rats. Individual points here and onward indicate animal averages. Here and below, CTL: n=8, XPro: n=8. Wilcoxon Rank Sum, $p=0.7$.

J. Average time to capture, K. latency to attack, and L. pursuit duration on Probe Day. Wilcoxon Rank Sum, time to capture, $p=0.0004$; latency to attack, $p=0.04$; pursuit duration, $p=0.01$.